Hindawi Publishing Corporation
EURASIP Journal on Advances in Signal Processing
Volume 2007, Article ID 83858, 18 pages
doi:10.1155/2007/83858

Research Article

Design of Optimal Quincunx Filter Banks for Image Coding

Yi Chen, Michael D. Adams, and Wu-Sheng Lu

Department of Electrical and Computer Engineering, University of Victoria, Victoria, BC, Canada V8W 3P6

Received 31 December 2005; Revised 8 June 2006; Accepted 16 July 2006

Recommended by Ivan Selesnick

Two new optimization-based methods are proposed for the design of high-performance quincunx filter banks for the application of image coding. These new techniques are used to build linear-phase finite-length-impulse-response (FIR) perfect-reconstruction (PR) systems with high coding gain, good frequency selectivity, and certain prescribed vanishing-moment properties. A parametrization of quincunx filter banks based on the lifting framework is employed to structurally impose the PR and linear-phase conditions. Then, the coding gain is maximized subject to a set of constraints on vanishing moments and frequency selectivity. Examples of filter banks designed using the newly proposed methods are presented and shown to be highly effective for image coding. In particular, our new optimal designs are shown to outperform three previously proposed quincunx filter banks in 72% to 95% of our experimental test cases. Moreover, in some limited cases, our optimal designs are even able to outperform the well-known (separable) 9/7 filter bank (from the JPEG-2000 standard).

1. INTRODUCTION

Filter banks have proven to be a highly effective tool for image coding applications [1]. In such applications, one typically desires filter banks to have perfect reconstruction (PR), linear-phase, high coding gain, good frequency selectivity, and satisfactory vanishing-moment properties. The PR property facilitates the construction of a lossless compression system. The linear-phase property is crucial to avoiding phase distortion. High coding gain leads to filter banks with good energy compaction capabilities. The presence of vanishing moments helps to reduce the number of nonzero coefficients in the highpass subbands and tends to lead to smoother synthesis basis functions. Good frequency selectivity serves to minimize aliasing in the subband signals. Designing nonseparable two-dimensional (2D) filter banks with all of the preceding properties is an extremely challenging task.

In the one-dimensional (1D) case, various filter-bank design techniques have been successfully developed. In the nonseparable 2D case, however, far fewer effective methods have been proposed. Variable transformation methods are commonly used for the design of 2D filter banks. With such methods, a 1D prototype filter bank is first designed, and then mapped into a 2D filter bank through a transformation of variables [2–6]. For example, the McClellan transformation [7] has been used in numerous design approaches. Other design techniques have also been proposed where a transformation is applied to the polyphase components of the filters instead of the original filter transfer functions [8–11]. These transformation-based designs have the restriction that one cannot explicitly control the shape of the 2D filter frequency responses. Moreover, in some cases, the transformed 2D filter banks can only achieve approximate PR. Direct optimization of the filter coefficients has also been proposed [12–14], but because of the involvement of large numbers of variables and nonlinear, nonconvex constraints, such optimization typically leads to a very complicated system, which is often difficult to solve. Designs utilizing the lifting framework [15, 16] have been proposed in [17, 18] for two-channel 2D filter banks with an arbitrary number of vanishing moments. With these methods, however, only interpolating filter banks are considered (i.e., filter banks with two lifting steps).

The Cayley transform has been used in the characterization and design of multidimensional orthogonal filter banks [19, 20]. In [21], B-spline filters and the McClellan transformation are used to construct orthogonal quincunx wavelets with fractional order of approximation. A technique utilizing polyharmonic B-splines is proposed in [22] for designing multidimensional/quincunx wavelet bases. Although the preceding design methods are interesting and certainly worthy of mention, they are not useful for the particular design

problem considered in our work. This is due to the fact that we consider the design of nontrivial linear-phase *finite-length-impulse-response* (FIR) PR filter banks. In the quincunx case, such filter banks cannot be orthogonal [23]. Furthermore, since we are interested in FIR filter banks, methods that yield filter banks with infinite-length-impulse-response (IIR) filters are not helpful either.

Uniform and nonuniform 2D directional filter banks are proposed in [24] to process images with better directional selectivity than conventional wavelets. Although we mention this development here for completeness, it addresses a different problem from that considered herein. In our work, we seek to design filter banks that can be used in a standard wavelet configuration. For this reason, methods for the design of directional filter banks, while interesting, are not applicable to the problem at hand.

In this paper, we propose two new optimization-based methods for constructing FIR quincunx filter banks with all of the aforementioned desirable properties (i.e., PR, linear-phase, high coding gain, good frequency selectivity, and certain vanishing-moments properties).

The rest of this paper is structured as follows. Section 2 briefly presents the notational conventions used herein. Then, Section 3 introduces quincunx filter banks, and Section 4 presents a parametrization of linear-phase PR quincunx filter banks based on the lifting framework. Optimal design algorithms for quincunx filter banks with two and more than two lifting steps are proposed in Sections 5 and 6, respectively. Several design examples are then presented in Section 7 and their effectiveness for image coding is demonstrated in Section 8. Finally, Section 9 concludes with a summary of our work and some closing remarks.

2. NOTATION AND TERMINOLOGY

Before proceeding further, a few comments are in order concerning the notation used herein. In this paper, the sets of integers and real numbers are denoted as $\mathbb{Z}$ and $\mathbb{R}$, respectively. The symbols $\mathbb{Z}^*$, $\mathbb{Z}^+$, $\mathbb{Z}^-$, $\mathbb{Z}_o$, and $\mathbb{Z}_e$ denote the sets of nonnegative, positive, negative, odd, and even integers, respectively. For $a \in \mathbb{R}$, $\lfloor a \rfloor$ denotes the largest integer no greater than a, and $\lceil a \rceil$ denotes the smallest integer no less than a. For $m, n \in \mathbb{Z}$, we define the mod function as $\mathrm{mod}(m, n) = m - n\lfloor m/n \rfloor$.

Matrices and vectors are denoted by upper- and lowercase boldface letters, respectively. The symbols $\mathbf{0}$, $\mathbf{1}$, and $\mathbf{I}$ are used to denote a vector/matrix of all zeros, a vector/matrix of all ones, and an identity matrix, respectively, the dimensions of which should be clear from the context. For matrix multiplication, we define the product notation as $\prod_{k=M}^{N} \mathbf{A}_k \triangleq \mathbf{A}_N \mathbf{A}_{N-1} \cdots \mathbf{A}_{M+1} \mathbf{A}_M$ for $N \geq M$. For convenience, a linear (or polynomial) function of the elements of a vector $\mathbf{x}$ is simply referred to as a linear (or polynomial) function in $\mathbf{x}$.

An element of a sequence x defined on $\mathbb{Z}^2$ is denoted either as $x[\mathbf{n}]$ or as $x[n_0, n_1]$ (whichever is more convenient), where $\mathbf{n} = [n_0 \;\; n_1]^T$ and $n_0, n_1 \in \mathbb{Z}$. Let $\mathbf{n} = [n_0 \;\; n_1]^T$ and let $\mathbf{z} = [z_0 \;\; z_1]^T$. Then, we define $|\mathbf{n}| = n_0 + n_1$ and $\mathbf{z}^{\mathbf{n}} = z_0^{n_0} z_1^{n_1}$. Furthermore, for a matrix $\mathbf{M} = [\mathbf{m}_0 \;\; \mathbf{m}_1]$ with $\mathbf{m}_k$ being the kth column of $\mathbf{M}$, we define $\mathbf{z}^{\mathbf{M}} = [\mathbf{z}^{\mathbf{m}_0} \;\; \mathbf{z}^{\mathbf{m}_1}]^T$. In the rest of this paper, unless otherwise noted, we will use $\mathbf{M}$ to denote the generating matrix $\left[\begin{smallmatrix} 1 & 1 \\ 1 & -1 \end{smallmatrix}\right]$ of the quincunx lattice. For convenience, we denote the partial derivative operator with respect to $\boldsymbol{\omega} = [\omega_0 \;\; \omega_1]^T$ as

$$\triangle^{\mathbf{n}} = \frac{\partial^{|\mathbf{n}|}}{\partial \omega_0^{n_0} \partial \omega_1^{n_1}}, \tag{1}$$

where $\mathbf{n} = [n_0 \;\; n_1]^T \in (\mathbb{Z}^*)^2$.

The Fourier transform of a sequence h is denoted as $\widehat{h}$. A (2D) filter H with impulse response h is said to be linear phase with group delay $\mathbf{c}$ if, for some $\mathbf{c} \in (1/2)\mathbb{Z}^2$, $h[\mathbf{n}] = h[2\mathbf{c} - \mathbf{n}]$ for all $\mathbf{n} \in \mathbb{Z}^2$. In passing, we note that the frequency response $\widehat{h}(\boldsymbol{\omega})$ of a linear-phase filter with impulse response h and group delay $\mathbf{c}$ can be expressed as

$$\widehat{h}(\boldsymbol{\omega}) = e^{-j\boldsymbol{\omega}^T \mathbf{c}} \sum_{\mathbf{n} \in \mathbb{Z}^2} h[\mathbf{n}] \cos\left[\boldsymbol{\omega}^T (\mathbf{n} - \mathbf{c})\right]. \tag{2}$$

For convenience, in what follows, we define the signed amplitude response $\widehat{h}_a(\boldsymbol{\omega})$ of H as

$$\widehat{h}_a(\boldsymbol{\omega}) = \sum_{\mathbf{n} \in \mathbb{Z}^2} h[\mathbf{n}] \cos\left[\boldsymbol{\omega}^T (\mathbf{n} - \mathbf{c})\right] \tag{3}$$

(i.e., the quantity $\widehat{h}_a(\boldsymbol{\omega})$ is $\widehat{h}(\boldsymbol{\omega})$ without the exponential factor $e^{-j\boldsymbol{\omega}^T \mathbf{c}}$). Thus, the magnitude response of H is trivially given by $|\widehat{h}_a(\boldsymbol{\omega})|$.

In image coding, the peak-signal-to-noise ratio (PSNR) is a commonly used measure for distortion. For an original image x and its reconstructed version x_r, the PSNR is defined as

$$\mathrm{PSNR} = 20 \log_{10} \left(\frac{2^P - 1}{\sqrt{\mathrm{MSE}}} \right), \tag{4}$$

where

$$\mathrm{MSE} = \frac{1}{N_0 N_1} \sum_{n_0=0}^{N_0-1} \sum_{n_1=0}^{N_1-1} \left(x_r[n_0, n_1] - x[n_0, n_1] \right)^2, \tag{5}$$

and each image has dimension $N_0 \times N_1$ and P bits/sample.

3. QUINCUNX FILTER BANKS

A quincunx filter bank has the canonical form shown in Figure 1. The filter bank consists of lowpass and highpass

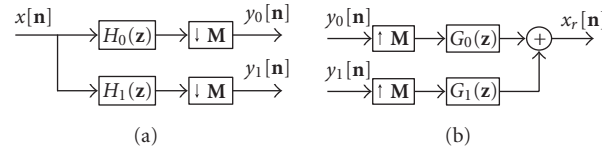

Figure 1: The canonical form of a quincunx filter bank: (a) analysis side, and (b) synthesis side.

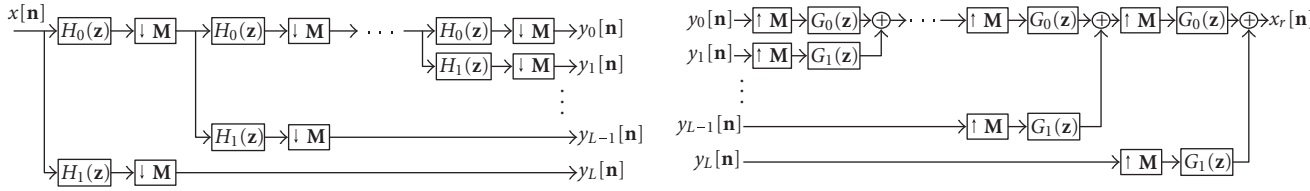

FIGURE 2: The structure of an L-level octave-band filter bank: (a) analysis side, and (b) synthesis side.

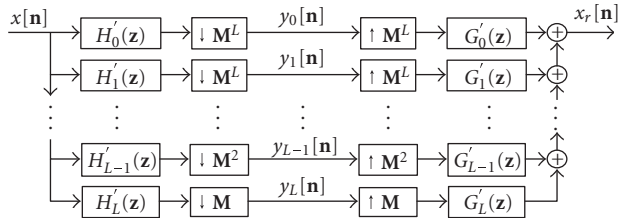

FIGURE 3: The equivalent nonuniform filter bank associated with the L-level octave-band filter bank.

analysis filters H_0 and H_1, lowpass and highpass synthesis filters G_0 and G_1, and $\mathbf{M}$-fold downsamplers and upsamplers.

In image coding applications, a quincunx filter bank is typically applied in a recursive manner, resulting in an octave-band filter-bank structure as shown in Figure 2. For an L-level octave-band filter bank generated from a quincunx filter bank with analysis filters $\{H_k\}$, the equivalent nonuniform filter bank has $L+1$ channels with analysis filters $\{H_i'\}$ and synthesis filters $\{G_i'\}$ as shown in Figure 3. The transfer functions $\{H_i'(\mathbf{z})\}$ of $\{H_i'\}$ are given by

$$H_i'(\mathbf{z}) = \begin{cases} \prod_{k=0}^{L-1} H_0(\mathbf{z}^{\mathbf{M}^k}), & i = 0, \\ H_1(\mathbf{z}^{\mathbf{M}^{L-i}}) \prod_{k=0}^{L-i-1} H_0(\mathbf{z}^{\mathbf{M}^k}), & 1 \le i \le L-1, \\ H_1(\mathbf{z}), & i = L. \end{cases} \tag{6}$$

The transfer functions $\{G_i'(\mathbf{z})\}$ of the equivalent synthesis filters $\{G_i'\}$ can be derived in a similar fashion.

4. LIFTING PARAMETRIZATION OF QUINCUNX FILTER BANKS

Rather than parameterizing a quincunx filter bank in terms of its canonical form, shown earlier in Figure 1, we instead employ the lifting framework [15, 16]. The lifting realization of a quincunx filter bank has the form shown in Figure 4. Essentially, the filter bank is realized in polyphase form, with the analysis and synthesis polyphase filtering each being performed by a ladder network consisting of 2λ lifting filters $\{A_k\}$. Without loss of generality, we may assume that none of the $\{A_k(\mathbf{z})\}$ are identically zero, except possibly $A_1(\mathbf{z})$ and $A_{2\lambda}(\mathbf{z})$.

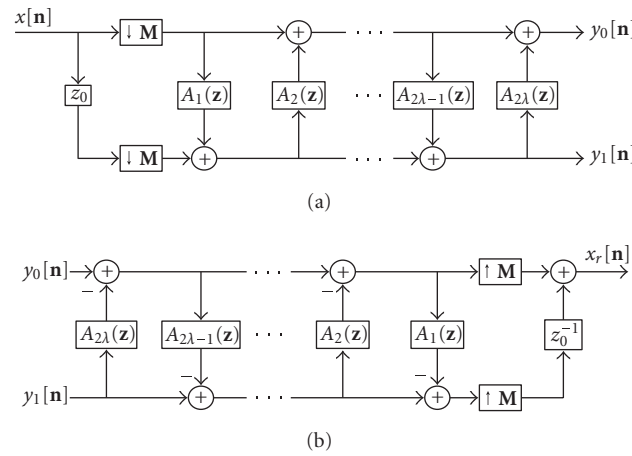

FIGURE 4: Lifting realization of a quincunx filter bank: (a) analysis side, and (b) synthesis side.

Given the lifting filters $\{A_k\}$, the corresponding analysis filter transfer functions $H_0(\mathbf{z})$ and $H_1(\mathbf{z})$ can be calculated as

$$\begin{bmatrix} H_0(\mathbf{z}) \\ H_1(\mathbf{z}) \end{bmatrix} = \begin{bmatrix} H_{0,0}(\mathbf{z}^{\mathbf{M}}) & H_{0,1}(\mathbf{z}^{\mathbf{M}}) \\ H_{1,0}(\mathbf{z}^{\mathbf{M}}) & H_{1,1}(\mathbf{z}^{\mathbf{M}}) \end{bmatrix} \begin{bmatrix} 1 \\ z_0 \end{bmatrix}, \tag{7}$$

where

$$\begin{bmatrix} H_{0,0}(\mathbf{z}) & H_{0,1}(\mathbf{z}) \\ H_{1,0}(\mathbf{z}) & H_{1,1}(\mathbf{z}) \end{bmatrix} = \prod_{k=1}^{\lambda} \left(\begin{bmatrix} 1 & A_{2k}(\mathbf{z}) \\ 0 & 1 \end{bmatrix} \begin{bmatrix} 1 & 0 \\ A_{2k-1}(\mathbf{z}) & 1 \end{bmatrix} \right). \tag{8}$$

The synthesis filter transfer functions $G_0(\mathbf{z})$ and $G_1(\mathbf{z})$ can then be trivially computed as $G_k(\mathbf{z}) = (-1)^{1-k} z_0^{-1} H_{1-k}(-\mathbf{z})$. Since the synthesis filters are completely determined by the analysis filters, we need only to consider the analysis side of the filter bank in what follows.

The use of the above lifting-based parametrization is helpful in several respects. First, the PR condition is automatically satisfied by such a parametrization. Second, the linear-phase condition can be imposed with relative ease, as we will see momentarily. Thus, the need for additional cumbersome constraints during optimization for PR and linear phase is eliminated. Lastly, the lifting realization trivially allows for the construction of reversible integer-to-integer mappings [25], which are often useful for image coding and are employed later in this work.

Now we further consider the linear-phase condition. As it turns out, the linear-phase condition can be satisfied with a prudent choice of lifting filters $\{A_k\}$. In particular, we have shown the below result.

Theorem 1 (sufficient condition for linear phase). *Consider a quincunx filter bank constructed from the lifting framework with 2λ lifting filters as shown in Figure 4(a). If each lifting filter A_k is symmetric with its group delay $\mathbf{c}_k$ satisfying*

$$\mathbf{c}_k = (-1)^k \begin{bmatrix} \frac{1}{2} & \frac{1}{2} \end{bmatrix}^T, \tag{9}$$

then the analysis filters H_0 and H_1 are symmetric with group delays $[0 \;\; 0]^T$ and $[-1 \;\; 0]^T$, respectively.

A proof of the preceding theorem is provided in the first author's thesis [26] but is omitted here for the sake of brevity. The significance of Theorem 1 is that the linear-phase condition can be trivially satisfied by choosing the lifting filters to have certain symmetry properties.

Now, we examine the relationship between the analysis filter frequency responses and the lifting-filter coefficients. Since the lifting filter A_k has linear phase with group delay $\mathbf{c}_k = (-1)^k[1/2 \;\; 1/2]^T$, the support region of A_k is a rectangle of size $2l_{k,0} \times 2l_{k,1}$ for some $l_{k,0}, l_{k,1} \in \mathbb{Z}^+$, and the number of independent coefficients of A_k is $2l_{k,0}l_{k,1}$. Let $\mathbf{a}_k$ be a vector containing the independent coefficients of A_k. Then, there are $2l_{k,0}l_{k,1}$ elements in $\mathbf{a}_k$ indexed from 0 to $2l_{k,0}l_{k,1} - 1$.

Consider an odd-indexed lifting filter A_{2k-1}. Its support region can be expressed as $\{-l_{2k-1,0}, -l_{2k-1,0}+1, \ldots, l_{2k-1,0} - 1\} \times \{-l_{2k-1,1}, -l_{2k-1,1}+1, \ldots, l_{2k-1,1}-1\}$. The nth element of the coefficient vector $\mathbf{a}_{2k-1}$ is defined as $a_{2k-1}[n_0, n_1]$ with n_0 and n_1 given by

$$\begin{aligned} n_0 &= \left\lfloor \frac{n}{(2l_{2k-1,1})} \right\rfloor \in \{0, 1, \ldots, l_{2k-1,0} - 1\}, \\ n_1 &= \bmod (n, 2l_{2k-1,1}) \\ &\quad - l_{2k-1,1} \in \{ -l_{2k-1,1}, -l_{2k-1,1}+1, \ldots, l_{2k-1,1} - 1\}. \end{aligned} \tag{10}$$

Since A_{2k-1} has linear phase, the frequency response of A_{2k-1} can be written from (2) as

$$\begin{aligned} \hat{a}_{2k-1}(\boldsymbol{\omega}) &= e^{-j\boldsymbol{\omega}^T \mathbf{c}_{2k-1}} \sum_{\mathbf{n} \in \mathbb{Z}^2} a_{2k-1}[\mathbf{n}] \cos\left[\boldsymbol{\omega}^T (\mathbf{n} - \mathbf{c}_{2k-1})\right] \\ &= 2e^{j(1/2)(\omega_0+\omega_1)} \sum_{n_0=0}^{l_{2k-1,0}-1} \sum_{n_1=-l_{2k-1,1}}^{l_{2k-1,1}-1} a_{2k-1}[n_0, n_1] \\ &\quad \times \cos\left[\omega_0\left(n_0 + \frac{1}{2}\right) + \omega_1\left(n_1 + \frac{1}{2}\right)\right]. \end{aligned} \tag{11}$$

In the upsampled domain, $\hat{a}_{2k-1}(\mathbf{M}^T\boldsymbol{\omega})$ can then be expressed as

$$\begin{aligned} \hat{a}_{2k-1}(\mathbf{M}^T\boldsymbol{\omega}) &= 2e^{j\omega_0} \sum_{n_0=0}^{l_{2k-1,0}-1} \sum_{n_1=-l_{2k-1,1}}^{l_{2k-1,1}-1} a_{2k-1}[n_0, n_1] \\ &\quad \times \cos\left[\omega_0(n_0 + n_1 + 1) + \omega_1(n_0 - n_1)\right]. \end{aligned} \tag{12}$$

Thus, $\hat{a}_{2k-1}(\mathbf{M}^T\boldsymbol{\omega})$ can be compactly written as

$$\hat{a}_{2k-1}(\mathbf{M}^T\boldsymbol{\omega}) = e^{j\omega_0} \mathbf{a}_{2k-1}^T \mathbf{v}_{2k-1}, \tag{13}$$

where $\mathbf{v}_{2k-1}$ is a vector of $2l_{2k-1,0}l_{2k-1,1}$ elements indexed from 0 to $2l_{2k-1,0}l_{2k-1,1} - 1$, and the nth element of $\mathbf{v}_{2k-1}$ is given by

$$\mathbf{v}_{2k-1}[n] = 2\cos\left[\omega_0(n_0 + n_1 + 1) + \omega_1(n_0 - n_1)\right] \tag{14}$$

with n_0 and n_1 given by (10).

Now, consider an even-indexed lifting filter A_{2k}. Its support region is $\{-l_{2k,0}+1, -l_{2k,0}+2, \ldots, l_{2k,0}\} \times \{-l_{2k,1}+1, -l_{2k,1}+2, \ldots, l_{2k,1}\}$. The nth element of the coefficient vector $\mathbf{a}_{2k}$ is defined as $a_{2k}[n_0, n_1]$ with n_0 and n_1 given by

$$\begin{aligned} n_0 &= \left\lfloor \frac{n}{(2l_{2k,1})} \right\rfloor + 1 \in \{1, 2, \ldots, l_{2k,0}\}, \\ n_1 &= \bmod (n, 2l_{2k,1}) \\ &\quad - l_{2k,1} + 1 \in \{ -l_{2k,1}+1, -l_{2k,1}+2, \ldots, l_{2k,1}\}, \end{aligned} \tag{15}$$

respectively. The frequency response $\hat{a}_{2k}(\boldsymbol{\omega})$ of A_{2k} is computed as

$$\begin{aligned} \hat{a}_{2k}(\boldsymbol{\omega}) &= 2e^{-j(1/2)(\omega_0+\omega_1)} \sum_{n_0=1}^{l_{2k,0}} \sum_{n_1=1-l_{2k,1}}^{l_{2k,1}} a_{2k}[n_0, n_1] \\ &\quad \times \cos\left[\omega_0\left(n_0 - \frac{1}{2}\right) + \omega_1\left(n_1 - \frac{1}{2}\right)\right]. \end{aligned} \tag{16}$$

In the upsampled domain, $\hat{a}_{2k}(\mathbf{M}^T\boldsymbol{\omega})$ can be expressed as

$$\hat{a}_{2k}(\mathbf{M}^T\boldsymbol{\omega}) = e^{-j\omega_0} \mathbf{a}_{2k}^T \mathbf{v}_{2k}, \tag{17}$$

where $\mathbf{v}_{2k}$ is a vector of $2l_{2k,0}l_{2k,1}$ elements indexed from 0 to $2l_{2k,0}l_{2k,1} - 1$, and the nth element of $\mathbf{v}_{2k}$ is defined as

$$\mathbf{v}_{2k}[n] = 2\cos\left[\omega_0(n_0 + n_1 - 1) + \omega_1(n_0 - n_1)\right] \tag{18}$$

with n_0 and n_1 given by (15).

Rewriting (7) and (8) in the Fourier domain, we have

$$\begin{bmatrix} \hat{h}_0(\boldsymbol{\omega}) \\ \hat{h}_1(\boldsymbol{\omega}) \end{bmatrix} = \begin{bmatrix} \hat{h}_{0,0}(\mathbf{M}^T\boldsymbol{\omega}) & \hat{h}_{0,1}(\mathbf{M}^T\boldsymbol{\omega}) \\ \hat{h}_{1,0}(\mathbf{M}^T\boldsymbol{\omega}) & \hat{h}_{1,1}(\mathbf{M}^T\boldsymbol{\omega}) \end{bmatrix} \begin{bmatrix} 1 \\ e^{j\omega_0} \end{bmatrix}, \tag{19}$$

$$\begin{bmatrix} \hat{h}_{0,0}(\boldsymbol{\omega}) & \hat{h}_{0,1}(\boldsymbol{\omega}) \\ \hat{h}_{1,0}(\boldsymbol{\omega}) & \hat{h}_{1,1}(\boldsymbol{\omega}) \end{bmatrix} = \prod_{k=1}^{\lambda} \left(\begin{bmatrix} 1 & \hat{a}_{2k}(\boldsymbol{\omega}) \\ 0 & 1 \end{bmatrix} \begin{bmatrix} 1 & 0 \\ \hat{a}_{2k-1}(\boldsymbol{\omega}) & 1 \end{bmatrix} \right), \tag{20}$$

respectively. Substituting (13), (17), and (20) into (19), we obtain the frequency responses of the analysis filters as

$$\begin{aligned} \begin{bmatrix} \hat{h}_0(\boldsymbol{\omega}) \\ \hat{h}_1(\boldsymbol{\omega}) \end{bmatrix} &= \left(\prod_{k=1}^{\lambda} \left(\begin{bmatrix} 1 & e^{-j\omega_0} \mathbf{a}_{2k}^T \mathbf{v}_{2k} \\ 0 & 1 \end{bmatrix} \right.\right. \\ &\quad \left.\left. \times \begin{bmatrix} 1 & 0 \\ e^{j\omega_0} \mathbf{a}_{2k-1}^T \mathbf{v}_{2k-1} & 1 \end{bmatrix} \right) \right) \begin{bmatrix} 1 \\ e^{j\omega_0} \end{bmatrix}. \end{aligned} \tag{21}$$

We further define a vector $\mathbf{x}$ containing all of the independent coefficients $\{\mathbf{a}_k\}$ of the lifting filters $\{A_k\}$ as

$$\mathbf{x} = \begin{bmatrix} \mathbf{a}_1^T & \mathbf{a}_2^T & \cdots & \mathbf{a}_{2\lambda}^T \end{bmatrix}^T. \tag{22}$$

Thus, $\mathbf{x}$ has $l_x = 2\sum_{i=1}^{2\lambda} l_{i,0}l_{i,1}$ elements. Clearly, each vector $\mathbf{a}_k$ can be expressed in terms of $\mathbf{x}$ as

$$\mathbf{a}_k = \underbrace{\begin{bmatrix}\mathbf{0}_{2l_{k,0}l_{k,1}\times\alpha_0} & \mathbf{I}_{2l_{k,0}l_{k,1}} & \mathbf{0}_{2l_{k,0}l_{k,1}\times\beta_0}\end{bmatrix}}_{\mathbf{E}_k}\mathbf{x} = \mathbf{E}_k\mathbf{x}, \tag{23}$$

where $\alpha_0 = 2\sum_{i=1}^{k-1} l_{i,0}l_{i,1}$ and $\beta_0 = 2\sum_{i=k+1}^{2\lambda} l_{i,0}l_{i,1}$. Substituting (23) into (21), we have

$$\begin{bmatrix}\widehat{h}_0(\boldsymbol{\omega})\\ \widehat{h}_1(\boldsymbol{\omega})\end{bmatrix} = \left(\prod_{k=1}^{\lambda}\left(\begin{bmatrix}1 & e^{-j\omega_0}\mathbf{x}^T\mathbf{E}_{2k}^T\mathbf{v}_{2k}\\ 0 & 1\end{bmatrix} \times \begin{bmatrix}1 & 0\\ e^{j\omega_0}\mathbf{x}^T\mathbf{E}_{2k-1}^T\mathbf{v}_{2k-1} & 1\end{bmatrix}\right)\right)\begin{bmatrix}1\\ e^{j\omega_0}\end{bmatrix}. \tag{24}$$

By expanding the preceding equation, each of the analysis filter frequency responses can be viewed as a polynomial in $\mathbf{x}$, the order of which depends on the number of lifting steps.

5. DESIGN OF FILTER BANKS WITH TWO LIFTING STEPS

Consider a quincunx filter bank as shown in Figure 4(a) with two lifting steps (i.e., $\lambda = 1$). As explained earlier, for image coding applications, we seek a filter bank with PR, linear-phase, high coding gain, good frequency selectivity, and certain vanishing-moment properties. To satisfy both the PR and linear-phase conditions, we use the lifting-based parametrization from Theorem 1. Having elected the use of a lifting-based parametrization for optimization purposes, we must now determine the relationships between the lifting-filter coefficients and the other desirable properties (such as high coding gain, good frequency selectivity, and certain vanishing-moment properties). In the sections that follow, these relationships are examined in more detail.

5.1. Coding gain

We begin by considering the relationship between the lifting-filter coefficients and coding gain. Coding gain is a measure of the energy compaction ability of a filter bank, and is defined as the ratio between the reconstruction error variance obtained by quantizing a signal directly to that obtained by quantizing the corresponding subband coefficients using an optimal bit allocation strategy. For an L-level octave-band quincunx filter bank, the coding gain G_{SBC} [27] is computed as

$$G_{\text{SBC}} = \prod_{k=0}^{L}\left(\frac{\alpha_k}{A_kB_k}\right)^{\alpha_k}, \tag{25}$$

where

$$\begin{aligned} A_k &= \sum_{\mathbf{m}\in\mathbb{Z}^2}\sum_{\mathbf{n}\in\mathbb{Z}^2} h_k'[\mathbf{m}]h_k'[\mathbf{n}]r[\mathbf{m}-\mathbf{n}],\\ B_k &= \alpha_k\sum_{\mathbf{n}\in\mathbb{Z}^2} g_k'^2[\mathbf{n}],\\ \alpha_k &= \begin{cases}2^{-L} & \text{for } k=0,\\ 2^{-(L+1-k)} & \text{for } k=1,2,\ldots,L,\end{cases}\end{aligned} \tag{26}$$

$h_k'[\mathbf{n}]$ and $g_k'[\mathbf{n}]$ are the impulse responses of the equivalent analysis and synthesis filters H_k' and G_k' (given by (6)), respectively, and r is the normalized autocorrelation of the input. Depending on the source image model, r is given by

$$r[n_0,n_1] = \begin{cases}\rho^{|n_0|+|n_1|} & \text{for separable model,}\\ \rho\sqrt{n_0^2+n_1^2} & \text{for isotropic model,}\end{cases} \tag{27}$$

where ρ is the correlation coefficient (typically, $0.90 \le \rho \le 0.95$). Due to the relationship between $\{h_k'[\mathbf{n}]\}$, $\{g_k'[\mathbf{n}]\}$, and the lifting-filter coefficient vector $\mathbf{x}$, the coding gain is a nonlinear function of $\mathbf{x}$.

5.2. Vanishing moments

Now, let us consider the relationship between the lifting-filter coefficients and vanishing moments. For a quincunx filter bank, the number of vanishing moments is equivalent to the order of zero at $[0\ \ 0]^T$ or $[\pi\ \ \pi]^T$ in the highpass or lowpass filter frequency response, respectively. For a linear-phase filter H with group delay $\mathbf{d} \in \mathbb{Z}^2$, its frequency response $\widehat{h}(\boldsymbol{\omega})$ can be computed by (2). The $\mathbf{m}$th-order partial derivative of its signed amplitude response $\widehat{h}_a(\boldsymbol{\omega})$ defined in (3) is then given by

$$\triangle^{\mathbf{m}}\widehat{h}_a(\boldsymbol{\omega}) = \begin{cases}(-1)^{|\mathbf{m}|/2}\displaystyle\sum_{\mathbf{n}\in\mathbb{Z}^2} h[\mathbf{n}](\mathbf{n}-\mathbf{d})^{\mathbf{m}} \\ \quad\times\cos\left[\boldsymbol{\omega}^T(\mathbf{n}-\mathbf{d})\right] & \text{for } |\mathbf{m}|\in\mathbb{Z}_e,\\ (-1)^{(|\mathbf{m}|+1)/2}\displaystyle\sum_{\mathbf{n}\in\mathbb{Z}^2} h[\mathbf{n}](\mathbf{n}-\mathbf{d})^{\mathbf{m}} \\ \quad\times\sin\left[\boldsymbol{\omega}^T(\mathbf{n}-\mathbf{d})\right] & \text{otherwise,}\end{cases} \tag{28}$$

where $\mathbf{m} = [m_0\ \ m_1]^T$. From the above equation, it follows that when $|\mathbf{m}| \in \mathbb{Z}_o$, the $\mathbf{m}$th-order partial derivative of $\widehat{h}_a(\boldsymbol{\omega})$ is automatically zero at $[0\ \ 0]^T$ and $[\pi\ \ \pi]^T$. Therefore, in order to have an Nth-order zero at $\boldsymbol{\omega} = [0\ \ 0]^T$, the filter coefficients need only satisfy

$$\sum_{\mathbf{n}\in\mathbb{Z}^2} h[\mathbf{n}](\mathbf{n}-\mathbf{d})^{\mathbf{m}} = 0 \quad \forall\,|\mathbf{m}|\in\mathbb{Z}_e \text{ such that } |\mathbf{m}| < N. \tag{29}$$

Similarly, in order to have an Nth-order zero at $\boldsymbol{\omega} = [\pi\ \ \pi]^T$, the filter coefficients need only satisfy

$$\sum_{\mathbf{n}\in\mathbb{Z}^2}(-1)^{|\mathbf{n}-\mathbf{d}|}h[\mathbf{n}](\mathbf{n}-\mathbf{d})^{\mathbf{m}} = 0 \quad \forall\,|\mathbf{m}|\in\mathbb{Z}_e \text{ such that } |\mathbf{m}| < N. \tag{30}$$

Since we only need to consider the case with $|\mathbf{m}| \in \mathbb{Z}_e$ in (29) and (30), the number of linear equations is $\lceil N/2\rceil^2$. Thus, for a filter bank to have $\widetilde{N}$ dual and N primal vanishing moments, the analysis filter coefficients are required to satisfy equations like those shown in (29) and (30). Since we use a lifting-based parametrization, the relationships need to be expressed in terms of the lifting-filter coefficients.

For a quincunx filter bank constructed with two lifting filters A_1 and A_2 as shown in Figure 4(a) with $\lambda = 1$, the constraints on vanishing moments form a linear system of equations in the lifting-filter coefficients. In order for this filter bank to have $\widetilde{N}$ dual and N primal vanishing moments, the impulse responses $a_1[\mathbf{n}]$ and $a_2[\mathbf{n}]$ of the lifting filters A_1 and A_2, respectively, should satisfy

$$\sum_{\mathbf{n}\in\mathbb{Z}^2} a_1[\mathbf{n}](-\mathbf{n})^{\mathbf{m}} = -\boldsymbol{\tau}_1^{\mathbf{m}}, \quad \forall \mathbf{m} \in (\mathbb{Z}^*)^2 \text{ with } |\mathbf{m}| < \widetilde{N}, \tag{31}$$

$$\sum_{\mathbf{n}\in\mathbb{Z}^2} a_2[\mathbf{n}](-\mathbf{n})^{\mathbf{m}} = \frac{1}{2}\boldsymbol{\tau}_2^{\mathbf{m}}, \quad \forall \mathbf{m} \in (\mathbb{Z}^*)^2 \text{ with } |\mathbf{m}| < N, \tag{32}$$

where $\boldsymbol{\tau}_1 = [1/2 \;\; 1/2]^T$ and $\boldsymbol{\tau}_2 = -\boldsymbol{\tau}_1 = [-1/2 \;\; -1/2]^T$ [18]. The total number of equations in (31) and (32) combined is $\binom{\widetilde{N}+1}{2} + \binom{N+1}{2} = ((\widetilde{N}+1)\widetilde{N} + (N+1)N)/2$.

The above results on vanishing moments can be applied to the filter banks from Theorem 1, where the lifting filters have linear phase. The support region of A_1 is $\{-l_{1,0}, -l_{1,0}+1, \ldots, l_{1,0}-1\} \times \{-l_{1,1}, -l_{1,1}+1, \ldots, l_{1,1}-1\}$ for some $l_{1,0}, l_{1,1} \in \mathbb{Z}$. Then, (31) can be rewritten as

$$\sum_{\substack{\mathbf{n}\in\{0,\ldots,l_{1,0}-1\} \\ \times\{-l_{1,1},\ldots,l_{1,1}-1\}}} a_1[\mathbf{n}]\left[(\mathbf{n}+\mathbf{1})^{\mathbf{m}} + (-\mathbf{n})^{\mathbf{m}}\right] = -2^{-|\mathbf{m}|}, \tag{33}$$

for $\mathbf{m} \in (\mathbb{Z}^*)^2$ and $|\mathbf{m}| < \widetilde{N}$. As previously discussed, we only need to consider the case with $|\mathbf{m}| \in \mathbb{Z}_e$. Therefore, the number of equations in (33) can be reduced to $\lceil \widetilde{N}/2 \rceil^2$. If we use $\mathbf{a}_1$ to denote the independent coefficients of A_1, the set of linear equations in (33) can be expressed in a more compact form as

$$\mathbf{A}_1\mathbf{a}_1 = \mathbf{b}_1, \tag{34}$$

where $\mathbf{A}_1$ is an $M_0 \times M_1$ matrix with $M_0 = \lceil \widetilde{N}/2 \rceil^2$ and $M_1 = 2l_{1,0}l_{1,1}$, and $\mathbf{b}_1$ is a vector with $\lceil \widetilde{N}/2 \rceil^2$ elements. Each element of $\mathbf{A}_1$ assumes the form $(\mathbf{n}+\mathbf{1})^{\mathbf{m}} + (-\mathbf{n})^{\mathbf{m}}$, and each element of $\mathbf{b}_1$ assumes the form $-2^{-|\mathbf{m}|}$.

Similarly, because of the linear-phase property of the second lifting filter A_2, (32) becomes

$$\sum_{\substack{\mathbf{n}\in\{1,\ldots,l_{2,0}\} \\ \times\{-l_{2,1}+1,\ldots,l_{2,1}\}}} a_2[\mathbf{n}]\left[(\mathbf{n}-\mathbf{1})^{\mathbf{m}} + (-\mathbf{n})^{\mathbf{m}}\right] = -(-2)^{-|\mathbf{m}|-1}, \tag{35}$$

for $\mathbf{m} \in (\mathbb{Z}^*)^2$, $|\mathbf{m}| \in \mathbb{Z}_e$, and $|\mathbf{m}| < N$. With $\mathbf{a}_2$ denoting the $2l_{2,0}l_{2,1}$ independent coefficients of A_2, (35) can be rewritten as

$$\mathbf{A}_2\mathbf{a}_2 = \mathbf{b}_2, \tag{36}$$

where $\mathbf{A}_2$ is an $M_0 \times M_1$ matrix with $M_0 = \lceil N/2 \rceil^2$ and $M_1 = 2l_{2,0}l_{2,1}$, and $\mathbf{b}_2$ is a vector with $\lceil N/2 \rceil^2$ elements. Elements of $\mathbf{A}_2$ and $\mathbf{b}_2$ assume the forms of $(\mathbf{n}-\mathbf{1})^{\mathbf{m}} + (-\mathbf{n})^{\mathbf{m}}$ and $-(-2)^{-|\mathbf{m}|-1}$, respectively.

Combining (34) and (36), we have the linear system of equations involving the lifting-filter coefficient vector $\mathbf{x}$ given by

$$\mathbf{A}\mathbf{x} = \mathbf{b}, \tag{37}$$

where $\mathbf{A} = \left[\begin{smallmatrix} \mathbf{A}_1 & \mathbf{0} \\ \mathbf{0} & \mathbf{A}_2 \end{smallmatrix}\right]$, $\mathbf{x} = \left[\begin{smallmatrix} \mathbf{a}_1 \\ \mathbf{a}_2 \end{smallmatrix}\right]$, and $\mathbf{b} = \left[\begin{smallmatrix} \mathbf{b}_1 \\ \mathbf{b}_2 \end{smallmatrix}\right]$. The number of equations in (37) is $\lceil \widetilde{N}/2 \rceil^2 + \lceil N/2 \rceil^2$.

It is worth noting that for a linear-phase filter bank with two lifting steps, the analysis filter frequency responses have some special properties if this filter bank has at least one dual vanishing moment. In particular, we have the result below.

Theorem 2 (filter banks with two lifting steps). *Consider a filter bank with two lifting steps satisfying Theorem 1. Let $\widehat{h}_0(\boldsymbol{\omega})$ and $\widehat{h}_1(\boldsymbol{\omega})$ be the frequency responses of the lowpass and highpass analysis filters H_0 and H_1, respectively. If this filter bank has at least one dual vanishing moment, then*

$$\widehat{h}_0(0,0) = 1, \tag{38a}$$

$$\widehat{h}_1(\pi,\pi) = -2 \tag{38b}$$

(i.e., the DC gain of the lowpass analysis filter H_0 is one and the Nyquist gain of the highpass analysis filter H_1 is two).

A proof of the above theorem is omitted here, but again can be found in the first author's thesis [26].

In the preceding discussion for filter banks with two lifting steps, it is assumed that the number of dual vanishing moments is no less than that of the primal ones (i.e., $\widetilde{N} \geq N$). This is desirable in the case of image coding, as the dual vanishing moments are more important than the primal ones for reducing the number of nonzero coefficients in the highpass subbands by annihilating polynomials. Furthermore, the presence of dual vanishing moments usually leads to smoother synthesis scaling and wavelet functions, which help to improve the subjective quality of the reconstructed images.

5.3. Frequency response

For image coding, we desire analysis filters with good frequency selectivity. Since a lifting-based parametrization of quincunx filter banks is employed, we consider the relationship between analysis filter frequency selectivity and the lifting filter coefficients.

To quantify the frequency selectivity of the filter bank, we measure the deviation in frequency response between an analysis filter H and an ideal filter H_d. In particular, we define the weighted frequency response error function e_h of H as

$$e_h = \int_{[-\pi,\pi)^2} W(\boldsymbol{\omega}) \left| \widehat{h}_a(\boldsymbol{\omega}) - D\widehat{h}_d(\boldsymbol{\omega}) \right|^2 d\boldsymbol{\omega}, \tag{39}$$

where $W(\boldsymbol{\omega})$ is a weighting function defined on $[-\pi,\pi)^2$, $\widehat{h}_a(\boldsymbol{\omega})$ is the signed amplitude response of H as defined by (3), $\widehat{h}_d(\boldsymbol{\omega})$ is the frequency response of the ideal filter H_d, and D is a scaling factor. In order for the filter H to approximate

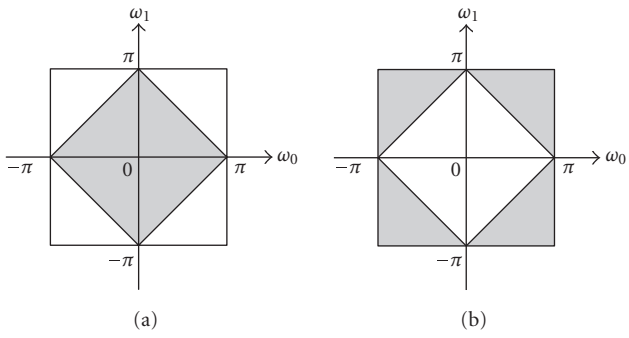

Figure 5: Ideal frequency responses of quincunx filter banks for the (a) lowpass filters and (b) highpass filters, where the shaded and unshaded areas represent the passband and stopband, respectively.

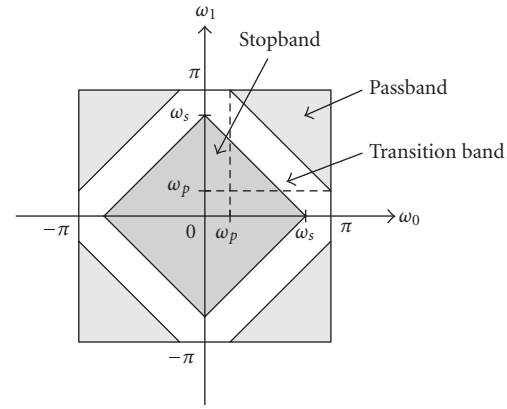

Figure 6: Weighting function for a highpass filter with diamond-shaped stopband.

the ideal filter, the frequency response error function e_h is required to satisfy

$$e_h \le \delta_h, \tag{40}$$

where δ_h is a prescribed upper bound on the error.

For a quincunx filter bank with sampling matrix $\mathbf{M} = \left[\begin{smallmatrix} 1 & 1 \\ 1 & -1 \end{smallmatrix}\right]$, the shape of filter passband is not unique [3, 17]. Herein, in order to match the human visual system, we use diamond-shaped ideal passband/stopband for the analysis and synthesis filters [28]. Figure 5(a) illustrates the ideal lowpass filter frequency response given by

$$\hat{h}_{0d}(\boldsymbol{\omega}) = \begin{cases} 1 & \text{for } |\omega_0 \pm \omega_1| \le \pi, \\ 0 & \text{otherwise,} \end{cases} \tag{41}$$

and Figure 5(b) depicts the ideal highpass filter frequency response given by

$$\hat{h}_{1d}(\boldsymbol{\omega}) = \begin{cases} 1 & \text{for } |\omega_0 \pm \omega_1| \ge \pi,\ \omega_0, \omega_1 \in [-\pi, \pi), \\ 0 & \text{otherwise.} \end{cases} \tag{42}$$

The weighting function $W(\boldsymbol{\omega})$ is used to control the relative importance of the passband and stopband. For a quincunx highpass filter with a diamond-shaped stopband, $W(\boldsymbol{\omega})$ is defined as

$$W(\boldsymbol{\omega}) = \begin{cases} 1 & \text{for passband } |\omega_0 \pm \omega_1| \ge \pi + \omega_p, \\ & \qquad \omega_0, \omega_1 \in [-\pi, \pi), \\ \gamma & \text{for stopband } |\omega_0 \pm \omega_1| \le \omega_s, \\ 0 & \text{otherwise (i.e., transition band),} \end{cases} \tag{43}$$

where $\gamma \ge 0$. By adjusting the value of γ, we can control the filter's performance in the stopband relative to the passband. In the case of highpass filters, for example, the weighting function is as depicted in Figure 6. The weighting function for a quincunx lowpass filter is defined in a similar way (i.e., with the roles of passband and stopband reversed in (43)).

Consider a filter bank as shown in Figure 4 with two lifting filters A_1 and A_2 satisfying Theorem 1. From (24), we obtain the frequency responses of the analysis filters as

$$\begin{bmatrix} \hat{h}_0(\boldsymbol{\omega}) \\ \hat{h}_1(\boldsymbol{\omega}) \end{bmatrix} = \begin{bmatrix} 1 & e^{-j\omega_0}\mathbf{x}^T\mathbf{E}_2^T\mathbf{v}_2 \\ 0 & 1 \end{bmatrix} \begin{bmatrix} 1 & 0 \\ e^{j\omega_0}\mathbf{x}^T\mathbf{E}_1^T\mathbf{v}_1 & 1 \end{bmatrix} \begin{bmatrix} 1 \\ e^{j\omega_0} \end{bmatrix}$$
$$= \begin{bmatrix} 1 + \mathbf{x}^T\mathbf{E}_2^T\mathbf{v}_2 + \mathbf{x}^T\mathbf{E}_2^T\mathbf{v}_2\mathbf{v}_1^T\mathbf{E}_1\mathbf{x} \\ e^{j\omega_0}\left(1 + \mathbf{x}^T\mathbf{E}_1^T\mathbf{v}_1\right) \end{bmatrix}. \tag{44}$$

Then, the signed amplitude response $\hat{h}_{1a}(\boldsymbol{\omega})$ of H_1 is

$$\hat{h}_{1a}(\boldsymbol{\omega}) = 1 + \mathbf{x}^T\mathbf{E}_1^T\mathbf{v}_1. \tag{45}$$

The frequency response error function of the highpass analysis filter H_1 is computed as

$$e_{h_1} = \int_{[-\pi,\pi)^2} W(\boldsymbol{\omega}) \left|\hat{h}_{1a}(\boldsymbol{\omega}) - D\hat{h}_{1d}(\boldsymbol{\omega})\right|^2 d\boldsymbol{\omega}, \tag{46}$$

where $W(\boldsymbol{\omega})$ is the weighting function defined in (43), $\hat{h}_{1d}(\boldsymbol{\omega})$ is the ideal frequency response of a quincunx highpass filter defined in (42), and the scaling factor D is chosen to be $D = 2$ in accordance with (38b). The frequency response error function in (46) can be expressed as the quadratic in the lifting-filter coefficient vector $\mathbf{x}$ given by

$$e_{h_1} = \mathbf{x}^T\mathbf{H}_x\mathbf{x} + \mathbf{x}^T\mathbf{s}_x + c_x, \tag{47}$$

where

$$\mathbf{H}_x = \int_{[-\pi,\pi)^2} W(\boldsymbol{\omega})\mathbf{E}_1^T\mathbf{v}_1\mathbf{v}_1^T\mathbf{E}_1\, d\boldsymbol{\omega},$$
$$\mathbf{s}_x = \int_{[-\pi,\pi)^2} 2W(\boldsymbol{\omega})\mathbf{E}_1^T\mathbf{v}_1\left[1 - 2\hat{h}_{1d}(\boldsymbol{\omega})\right] d\boldsymbol{\omega}, \tag{48}$$
$$c_x = \int_{[-\pi,\pi)^2} W(\boldsymbol{\omega})\left[1 - 2\hat{h}_{1d}(\boldsymbol{\omega})\right]^2 d\boldsymbol{\omega},$$

and $\mathbf{H}_x$ is a positive semidefinite matrix. Substituting (47) into the constraint on the frequency response (40), we obtain a quadratic inequality involving $\mathbf{x}$ as

$$\mathbf{x}^T\mathbf{H}_x\mathbf{x} + \mathbf{x}^T\mathbf{s}_x + c_x - \delta_h \le 0. \tag{49}$$

5.4. Design problem formulation

Consider a filter bank as shown in Figure 4(a) with two lifting steps. The design of such a filter bank with all of the desirable properties (i.e., PR, linear-phase, high coding gain, good frequency selectivity, and certain vanishing-moment properties) can be formulated as a constrained optimization problem. We employ the lifting-based parametrization introduced in Theorem 1. In this way, the PR and linear-phase conditions are automatically satisfied. We then maximize the coding gain subject to a set of constraints, which are chosen to ensure that the desired vanishing moment and frequency selectivity conditions are met. In what follows, we will show more precisely how this design problem can be formulated as a second-order cone programming (SOCP) problem.

In an SOCP problem, a linear function is minimized subject to a set of second-order cone constraints [29]. In other words, we have a problem of the following form:

$$\begin{aligned} &\text{minimize } \mathbf{f}^T\mathbf{x} \\ &\text{subject to } \|\mathbf{F}_i^T\mathbf{x}+\mathbf{c}_i\| \le \mathbf{f}_i^T\mathbf{x}+d_i \quad \text{for } i=1,\ldots,q, \end{aligned} \tag{50}$$

where $\mathbf{x}\in\mathbb{R}^n$ is the design vector containing n free variables, and $\mathbf{f}\in\mathbb{R}^n$, $\mathbf{F}_i\in\mathbb{R}^{n\times m_i}$, $\mathbf{c}_i\in\mathbb{R}^{m_i}$, $\mathbf{f}_i\in\mathbb{R}^n$, and $d_i\in\mathbb{R}$. The constraint $\|\mathbf{F}_i^T\mathbf{x}+\mathbf{c}_i\| \le \mathbf{f}_i^T\mathbf{x}+d_i$ is called a second-order cone constraint.

Consider a filter bank satisfying Theorem 1 with two lifting filters A_1 and A_2, having support sizes of $2l_{1,0}\times 2l_{1,1}$ and $2l_{2,0}\times 2l_{2,1}$, respectively. We use $\mathbf{x}$ to denote the vector consisting of the $2l_{1,0}l_{1,1}+2l_{2,0}l_{2,1}$ independent lifting-filter coefficients defined in (22). As explained previously, in terms of the lifting-filter coefficient vector $\mathbf{x}$, the constraint on vanishing moments is linear and the constraint on the frequency response of the highpass analysis filter is quadratic.

From Section 5.2, we know that in order for a filter bank to have N primal and $\widetilde{N}$ dual vanishing moments, $\mathbf{x}$ needs to be the solution of a system of $\lceil\widetilde{N}/2\rceil^2+\lceil N/2\rceil^2$ linear equations given by

$$\mathbf{A}\mathbf{x}=\mathbf{b}. \tag{51}$$

In (51), $\mathbf{A}\in\mathbb{R}^{m\times n}$ with rank r and $\mathbf{b}\in\mathbb{R}^{m\times 1}$, where $m=\lceil\widetilde{N}/2\rceil^2+\lceil N/2\rceil^2$, $n=2l_{1,0}l_{1,1}+2l_{2,0}l_{2,1}$, and $r\le\min\{m,n\}$. The system is underdetermined when there are enough lifting-filter coefficients such that $m<n$. In what follows, we assume that the system is underdetermined so that our eventual optimization problem will have a feasible region containing more than one point. Let the singular value decomposition (SVD) of $\mathbf{A}$ be $\mathbf{A}=\mathbf{U}\mathbf{S}\mathbf{V}^T$. All of the solutions to (51) can be parameterized as

$$\mathbf{x}=\underbrace{\mathbf{A}^+\mathbf{b}}_{\mathbf{x}_s}+\mathbf{V}_r\boldsymbol{\phi}=\mathbf{x}_s+\mathbf{V}_r\boldsymbol{\phi}, \tag{52}$$

where $\mathbf{A}^+$ is the Moore-Penrose pseudoinverse of $\mathbf{A}$, $\mathbf{V}_r=[\mathbf{v}_{r+1}\mathbf{v}_{r+2}\cdots\mathbf{v}_n]$ is a matrix composed of the last $n-r$ columns of $\mathbf{V}$, and $\boldsymbol{\phi}$ is an arbitrary $(n-r)$-dimensional vector. Henceforth, we will use $\boldsymbol{\phi}$ as the design vector instead of $\mathbf{x}$. Thus, the vanishing-moment condition is automatically satisfied for any choice of $\boldsymbol{\phi}$ and the number of free variables involved is reduced from n to $n-r$.

The design objective is to maximize the coding gain G_{SBC} of an L-level octave-band quincunx filter bank, which is computed by (25) and can be expressed as a nonlinear function of the design vector $\boldsymbol{\phi}$. Let $G=-10\log_{10}G_{\text{SBC}}$. Then, the problem of maximizing G_{SBC} is equivalent to minimizing G. Although taking the logarithm helps to improve the numerical stability of the optimization algorithm and reduces the nonlinearity in G, the direct minimization of G remains a very difficult task. Our design strategy is that, for a given parameter vector $\boldsymbol{\phi}$, we seek a small perturbation $\boldsymbol{\delta}_\phi$ such that $G(\boldsymbol{\phi}+\boldsymbol{\delta}_\phi)$ is reduced relative to $G(\boldsymbol{\phi})$. Because $\|\boldsymbol{\delta}_\phi\|$ is small, we can write the quadratic and linear approximations of $G(\boldsymbol{\phi}+\boldsymbol{\delta}_\phi)$, respectively, as

$$G(\boldsymbol{\phi}+\boldsymbol{\delta}_\phi)\approx G(\boldsymbol{\phi})+\mathbf{g}^T\boldsymbol{\delta}_\phi+\frac{1}{2}\boldsymbol{\delta}_\phi^T\mathbf{Q}\boldsymbol{\delta}_\phi, \tag{53}$$

$$G(\boldsymbol{\phi}+\boldsymbol{\delta}_\phi)\approx G(\boldsymbol{\phi})+\mathbf{g}^T\boldsymbol{\delta}_\phi, \tag{54}$$

where $\mathbf{g}$ and $\mathbf{Q}$ are, respectively, the gradient and the Hessian of $G(\boldsymbol{\phi})$ at the point $\boldsymbol{\phi}$. Having obtained such a $\boldsymbol{\delta}_\phi$ (subject to some additional constraints to be described shortly), the parameter vector $\boldsymbol{\phi}$ is updated to $\boldsymbol{\phi}+\boldsymbol{\delta}_\phi$. This iterative process continues until the reduction in G (i.e., $|G(\boldsymbol{\phi}+\boldsymbol{\delta}_\phi)-G(\boldsymbol{\phi})|$) becomes less than a prescribed tolerance ε.

Now, consider the constraint on the frequency response. In Section 5.3, we showed that for filter banks constructed with two lifting steps, the frequency response error function e_{h_1} of the highpass analysis filter H_1 is a quadratic polynomial in $\mathbf{x}$ as given by (47). Substituting (52) into (47), we have

$$e_{h_1}=\boldsymbol{\phi}^T\mathbf{H}_\phi\boldsymbol{\phi}+\boldsymbol{\phi}^T\mathbf{s}_\phi+c_\phi, \tag{55}$$

where

$$\begin{aligned} \mathbf{H}_\phi &= \mathbf{V}_r^T\mathbf{H}_x\mathbf{V}_r, \\ \mathbf{s}_\phi &= \mathbf{V}_r^T(\mathbf{H}_x+\mathbf{H}_x^T)\mathbf{x}_s+\mathbf{V}_r^T\mathbf{s}_x, \\ c_\phi &= \mathbf{x}_s^T\mathbf{H}_x\mathbf{x}_s+\mathbf{x}_s^T\mathbf{s}_x+c_x, \end{aligned} \tag{56}$$

and $\mathbf{H}_x$, $\mathbf{s}_x$, and c_x are given in (48). Moreover, it follows from the fact that $\mathbf{H}_x$ is positive semidefinite that $\mathbf{H}_\phi$ is also positive semidefinite. Now, let us replace $\boldsymbol{\phi}$ by $\boldsymbol{\phi}_k+\boldsymbol{\delta}_\phi$ and let the SVD of $\mathbf{H}_\phi$ be given by

$$\mathbf{H}_\phi=\mathbf{U}_H\boldsymbol{\Sigma}\mathbf{V}_H^T. \tag{57}$$

Then, (55) can also be written as

$$e_{h_1}=\|\widetilde{\mathbf{H}}_k\boldsymbol{\delta}_\phi+\widetilde{\mathbf{s}}_k\|^2+\widetilde{c}_k, \tag{58}$$

and the constraint (40) becomes the second-order cone constraint

$$\|\widetilde{\mathbf{H}}_k\boldsymbol{\delta}_\phi+\widetilde{\mathbf{s}}_k\|^2\le\delta_{h_1}-\widetilde{c}_k, \tag{59}$$

where

$$\begin{aligned} \widetilde{\mathbf{H}}_k &= \boldsymbol{\Sigma}^{1/2}\mathbf{U}_H^T, \\ \widetilde{\mathbf{s}}_k &= \frac{1}{2}\widetilde{\mathbf{H}}^{-T}(2\mathbf{H}_\phi\boldsymbol{\phi}_k+\mathbf{s}_\phi), \\ \widetilde{c}_k &= \boldsymbol{\phi}_k^T\mathbf{H}_\phi\boldsymbol{\phi}_k+\boldsymbol{\phi}_k^T\mathbf{s}_\phi+c_\phi-\|\widetilde{\mathbf{s}}_k\|^2. \end{aligned} \tag{60}$$

This iterative algorithm consists of the following steps (where k denotes the iteration number indexed from zero).

Step (1)

Compute $\mathbf{A}$ and $\mathbf{b}$ in (37) for the desired numbers of vanishing moments, and calculate $\mathbf{H}_\phi$, $\mathbf{s}_\phi$, and c_ϕ in (55). Then, select an initial point $\boldsymbol{\phi}_0$. This point can be chosen randomly, or chosen to be a quincunx filter bank proposed in [18]. The vanishing-moment condition is satisfied, and because of the way in which we choose the upper bound δ_{h_1} for the frequency response error function (to be discussed later), $\boldsymbol{\phi}_0$ will not violate the frequency response constraint. In this way, the initial point is in the feasible region.

Step (2)

For the kth iteration, at the point $\boldsymbol{\phi}_k$, compute the gradient $\mathbf{g}$ of $G(\boldsymbol{\phi})$ in (54), and calculate $\widetilde{\mathbf{H}}_k$, $\widetilde{\mathbf{s}}_k$, and $\widetilde{c}_k$ in (59). Then, solve the SOCP problem given by:

$$\begin{aligned} &\text{minimize } \mathbf{g}^T\boldsymbol{\delta}_\phi \\ &\text{subject to } ||\widetilde{\mathbf{H}}_k\boldsymbol{\delta}_\phi + \widetilde{\mathbf{s}}_k|| \le \sqrt{\delta_{h_1} - \widetilde{c}_k}, \\ &||\boldsymbol{\delta}_\phi|| \le \beta, \end{aligned} \tag{$p1$}$$

where β is a given small value used to ensure that the solution is within the vicinity of $\boldsymbol{\phi}_k$. Then, update $\boldsymbol{\phi}_k$ by $\boldsymbol{\phi}_{k+1} = \boldsymbol{\phi}_k + \gamma\boldsymbol{\delta}_\phi$, where γ is either chosen as one or determined by a line search explained in more detail later. A number of software packages are available for solving SOCP problems. In our work, for example, we use SeDuMi [30].

Step (3)

If $|G(\boldsymbol{\phi}_{k+1}) - G(\boldsymbol{\phi}_k)| < \varepsilon$, output $\boldsymbol{\phi}^* = \boldsymbol{\phi}_{k+1}$, compute $\mathbf{x}^* = \mathbf{x}_s + \mathbf{V}_r\boldsymbol{\phi}^*$, and stop. Otherwise, go to Step (2).

Algorithm 1: Two-lifting-step case.

Based on the preceding discussions, we now show how to employ the SOCP technique to solve the problem of maximizing the coding gain G_{SBC}, or equivalently minimizing G, with the vanishing-moment constraint $\mathbf{Ax} = \mathbf{b}$ as in (51) and the frequency response constraint $e_{h_1} \le \delta_{h_1}$ as in (40). This problem can be solved via Algorithm 1.

The vector $\mathbf{x}^*$ output by Algorithm 1 is then the optimal solution to this problem. The filter bank constructed from the lifting-filter coefficient vector $\mathbf{x}^*$ has high coding gain, good frequency selectivity, and the desired vanishing-moment properties (as well as PR and linear phase).

Two additional comments are now in order concerning the SOCP problem ($p1$) in the second step of the iterative algorithm (Algorithm 1). In particular, the choice of β is critical to the success of the algorithm. It should be chosen such that

$$\mathbf{g}^T\boldsymbol{\delta} \approx G(\boldsymbol{\phi} + \boldsymbol{\delta}) - G(\boldsymbol{\phi}) \quad \text{for } \|\boldsymbol{\delta}\| = \beta. \tag{61}$$

If β is too large, the linear approximation (54) is less accurate, resulting in the linear term $\mathbf{g}^T\boldsymbol{\delta}_\phi$ not correctly reflecting the actual reduction in G. If β is too small, in the kth iteration, the solution is restricted to an unnecessarily small region around $\boldsymbol{\phi}_k$, causing points outside this region which may provide a greater reduction in G to be excluded. For this reason, we incorporate a line search in Step (2) to find a better solution along the direction of $\boldsymbol{\delta}_\phi$. We first evaluate G at N_0 equally spaced points between $\boldsymbol{\phi}_k$ and $\boldsymbol{\phi}_k + \alpha\boldsymbol{\delta}_\phi$ along the direction of $\boldsymbol{\delta}_\phi$ for some $\alpha \ge 1$, including the point $\boldsymbol{\phi}_k + \boldsymbol{\delta}_\phi$. Then, we use the point $\boldsymbol{\phi}_k^*$ corresponding to the minimal G to select γ. By including a line search, in each iteration the reduction in G is as large as the reduction obtained without the line search. This makes the algorithm converges with less iterations. The choice of α depends on the choice of β. When β is large, we can choose $\alpha = 1$. When β is small, we can choose $\alpha \ge 1$. Note that a greater value of α may imply more evaluations of the coding gain function G in each iteration.

The second comment about Step (2) concerns the choice of the upper bound δ_{h_1} of the frequency response error function in the SOCP problem ($p1$). If δ_{h_1} is too small, the feasible region of the SOCP problem may be an empty set, especially for designs starting from a random initial point. Therefore, for the kth iteration, we choose δ_{h_1} to be a scaled version of the error function e_{h_1} evaluated at $\boldsymbol{\phi}_k$. That is, we select

$$\delta_{h_1} = d(\boldsymbol{\phi}_k^T\mathbf{H}_\phi\boldsymbol{\phi}_k + \boldsymbol{\phi}_k^T\mathbf{s}_\phi + c_\phi), \tag{62}$$

where $0 < d \le 1$ is a scaling factor. In this way, the error e_{h_1} is reduced after each iteration, and the frequency response of the highpass analysis filter H_1 improves gradually with each iteration.

5.5. Design algorithm with Hessian

In Algorithm 1, a linear approximation (54) of the coding gain function G is employed. This necessitates that the perturbation $\boldsymbol{\delta}_\phi$ be located in a small region. For this design problem, we can instead use the quadratic approximation in (53). In this way, the approximation accuracy can be improved, and the solution can be sought in a larger region. Algorithm 1 can be adapted to utilize the quadratic approximation with some minor changes to the SOCP problem in each iteration. In Step (2), we minimize $\mathbf{g}^T\boldsymbol{\delta}_\phi + (1/2)\boldsymbol{\delta}_\phi^T\mathbf{Q}\boldsymbol{\delta}_\phi$ instead of $\mathbf{g}^T\boldsymbol{\delta}_\phi$ in ($p1$). That is, we seek a solution to the following problem:

$$\begin{aligned} &\text{minimize } \mathbf{g}^T\boldsymbol{\delta}_\phi + \frac{1}{2}\boldsymbol{\delta}_\phi^T\mathbf{Q}\boldsymbol{\delta}_\phi \\ &\text{subject to } ||\widetilde{\mathbf{H}}\boldsymbol{\delta}_\phi + \widetilde{\mathbf{s}}|| \le \sqrt{\delta_{h_1} - \widetilde{c}}, \\ &||\boldsymbol{\delta}_\phi|| \le \beta. \end{aligned} \tag{63}$$

Let the SVD of $(1/2)\mathbf{Q}$ be $(1/2)\mathbf{Q} = \mathbf{U}_\mathbf{Q}\boldsymbol{\Sigma}_\mathbf{Q}\mathbf{V}_\mathbf{Q}^T$. When $\mathbf{Q}$ is positive semidefinite, we can rewrite the objective function as

$$\mathbf{g}^T\boldsymbol{\delta}_\phi + \frac{1}{2}\boldsymbol{\delta}_\phi^T\mathbf{Q}\boldsymbol{\delta}_\phi = ||\widetilde{\mathbf{Q}}\boldsymbol{\delta}_\phi + \widetilde{\mathbf{s}}_\mathbf{Q}||^2 + \widetilde{c}_Q, \tag{64}$$

where

$$\widetilde{\mathbf{Q}} = \boldsymbol{\Sigma}_\mathbf{Q}^{1/2}\mathbf{U}_\mathbf{Q}^T, \qquad \widetilde{\mathbf{s}}_\mathbf{Q} = \frac{1}{2}\widetilde{\mathbf{Q}}^{-T}\mathbf{g}, \qquad \widetilde{c}_Q = -\widetilde{\mathbf{s}}_\mathbf{Q}^T\widetilde{\mathbf{s}}_\mathbf{Q}. \tag{65}$$

Table 1: Comparison of algorithms with linear and quadratic approximations.

Filter bank	EX1	EX2
Approximation	Linear	Quadratic
One-level isotropic coding gain (dB)	6.86	6.86
Number of evaluations of G per iteration	10	65
Average time per iteration	0.4	1.0
Number of iterations	41	5
Total time (seconds)	20.1	5.1

If we further define $\widetilde{\boldsymbol{\delta}}_{\boldsymbol{\phi}} = [\eta \;\; \boldsymbol{\delta}_{\boldsymbol{\phi}}]^T$ and $\mathbf{f} = [1 \;\; 0 \;\; \cdots \;\; 0]^T$, then (63) becomes the SOCP problem,

$$\begin{aligned} &\text{minimize } \mathbf{f}^T\widetilde{\boldsymbol{\delta}}_{\boldsymbol{\phi}} \\ &\text{subject to } ||\widetilde{\widetilde{\mathbf{Q}}}\widetilde{\boldsymbol{\delta}}_{\boldsymbol{\phi}} + \widetilde{\mathbf{s}}_{\mathbf{Q}}|| \le \mathbf{f}^T\widetilde{\boldsymbol{\delta}}_{\boldsymbol{\phi}}, \\ &||\widetilde{\widetilde{\mathbf{H}}}\widetilde{\boldsymbol{\delta}}_{\boldsymbol{\phi}} + \widetilde{\mathbf{s}}|| \le \sqrt{\delta_{h_1} - \widetilde{c}}, \\ &||\widetilde{\mathbf{I}}\widetilde{\boldsymbol{\delta}}_{\boldsymbol{\phi}}|| \le \beta, \end{aligned} \tag{66}$$

where $\widetilde{\widetilde{\mathbf{Q}}} = [\mathbf{0} \;\; \widetilde{\mathbf{Q}}]$, $\widetilde{\widetilde{\mathbf{H}}} = [\mathbf{0} \;\; \widetilde{\mathbf{H}}]$, and $\widetilde{\mathbf{I}} = [\mathbf{0} \;\; \mathbf{I}]$.

Note that (64) holds only when $\mathbf{Q}$ is positive semidefinite and $\mathbf{Q}$ need not always be positive semidefinite. When $\mathbf{Q}$ is not positive semidefinite, however, we can simply revert to using a linear approximation.

When a quadratic approximation is employed, the algorithm reaches an optimal solution with fewer iterations than in the linear case, but takes longer for each iteration as the coding gain is evaluated many more times when computing the Hessian. To demonstrate this difference in behavior, we designed two filter banks, EX1 and EX2, using the original Algorithm 1 and the revised algorithm with the Hessian, respectively. Each optimization used the same initial point. This led to the results shown in Table 1. Clearly, very similar optimization results are obtained for these two designs in terms of the coding gain. For the design with the quadratic approximation, the time used for each iteration is increased compared to the linear-approximation case, but the number of iterations is reduced greatly, resulting in a much shorter overall time.

6. DESIGN OF FILTER BANKS WITH MORE THAN TWO LIFTING STEPS

Although Algorithm 1 only works for the two-lifting-step case, this algorithm can be generalized to design filter banks with more than two lifting steps. When more lifting filters are involved, however, the relationships between the filter-bank characteristics (i.e., coding gain, vanishing-moment properties, and frequency selectivity) and the lifting-filter coefficients become more complicated. In this section, we consider how to formulate the design as an SOCP problem based on these relationships.

The computation of the coding gain in this case is basically the same as the two-lifting-step case discussed in Section 5.1. For an L-level octave-band quincunx filter bank, the coding gain G_{SBC} is computed by (25), and G_{SBC} is a nonlinear function of the lifting-filter coefficients.

6.1. Vanishing moments

Compared to the two-lifting-step case, the vanishing-moments condition changes considerably for a filter bank as shown in Figure 4(a) with at least three lifting steps (i.e., $\lambda \ge 2$). The condition is no longer linear with respect to the lifting-filter coefficient vector $\mathbf{x}$. With the notations $\mathbf{a}_k$, $\mathbf{v}_k$, $\mathbf{x}$, and $\mathbf{E}_k$ introduced in Section 4, the frequency responses $\{\widehat{h}_k(\boldsymbol{\omega})\}$ of the analysis filters are given by (24), and $\{\widehat{h}_k(\boldsymbol{\omega})\}$ can each be expressed as a polynomial in $\mathbf{x}$.

In order for this filter bank to have $\widetilde{N}$ dual vanishing moments, the frequency response $\widehat{h}_1(\boldsymbol{\omega})$ of the highpass analysis filter should have an $\widetilde{N}$th-order zero at $[0 \;\; 0]^T$. Therefore, $\triangle^{\mathbf{m}}\widehat{h}_{1a}(0,0) = 0$ for all $\mathbf{m} \in (\mathbb{Z}^*)^2$ such that $|\mathbf{m}| \in \mathbb{Z}_e$ and $|\mathbf{m}| < \widetilde{N}$, where $\widehat{h}_{1a}(\boldsymbol{\omega})$ is the signed amplitude response of H_1 as defined in (3). As H_1 has linear phase and $\widehat{h}_1(\boldsymbol{\omega})$ can be viewed as a polynomial in $\mathbf{x}$, $\widehat{h}_{1a}(\boldsymbol{\omega})$, and thus $\widehat{h}_{1a}^{(\mathbf{m})}(0,0)$ can also be viewed as polynomials in $\mathbf{x}$. In this way, in order to have $\widetilde{N}$ dual vanishing moments, the lifting-filter coefficients in $\mathbf{x}$ need to satisfy $\lceil \widetilde{N}/2 \rceil^2$ polynomial equations. Similarly, in order to have N primal vanishing moments, the frequency response $\widehat{h}_0^{(\mathbf{m})}(\boldsymbol{\omega})$ of the lowpass analysis filter H_0 should satisfy $\triangle^{\mathbf{m}}\widehat{h}_{0a}(\pi,\pi) = 0$ for all $\mathbf{m} \in (\mathbb{Z}^*)^2$ such that $|\mathbf{m}| \in \mathbb{Z}_e$ and $|\mathbf{m}| < N$. It follows that $\mathbf{x}$ needs to satisfy $\lceil N/2 \rceil^2$ polynomial equations.

6.2. Frequency responses

Recall that in the two-lifting-step case, the frequency response constraint is defined in (39) and (40), and the constraint on the highpass analysis filter is a second-order cone. For filter banks with more than two lifting steps, we define the frequency response constraint in a similar way. The frequency response error functions of the lowpass and highpass analysis filters, however, are at least fourth-order polynomials in the lifting-filter coefficients. This is because the frequency responses of the analysis filters H_0 and H_1 are at least quadratic polynomials in the lifting-filter coefficient vector $\mathbf{x}$ when more than two lifting filters are involved.

6.3. Design problem formulation

In the two-lifting-step case, we saw that in terms of the lifting-filter coefficients, the vanishing-moment condition is a linear system of equations and the frequency response constraint is a second-order cone. For filter banks with more than two lifting steps, the design problem becomes increasingly complicated as the constraints on vanishing moments and frequency responses become higher-order polynomials in the lifting-filter coefficients. In order to use the SOCP technique, the constraints on vanishing moments and the frequency response must be approximated by linear and quadratic constraints, respectively.

We deal with the coding gain $G_{\mathrm{SBC}}(\mathbf{x})$ with the same strategy as in the two-lifting-step case. The linear approximation of G with $G(\mathbf{x}) = -10\log_{10} G_{\mathrm{SBC}}(\mathbf{x})$ is given by

$$G(\mathbf{x}+\boldsymbol{\delta}_{\mathbf{x}}) \approx G(\mathbf{x}) + \mathbf{g}^T\boldsymbol{\delta}_{\mathbf{x}}, \tag{67}$$

where $\mathbf{g}$ is the gradient of G at point $\mathbf{x}$. We iteratively seek a small perturbation $\boldsymbol{\delta}_{\mathbf{x}}$ in $\mathbf{x}$ such that $G(\mathbf{x}+\boldsymbol{\delta}_{\mathbf{x}})$ is reduced relative to $G(\mathbf{x})$ until the difference between $G(\mathbf{x}+\boldsymbol{\delta}_{\mathbf{x}})$ and $G(\mathbf{x})$ is less than a prescribed tolerance.

As discussed in Section 6.1, the constraint on vanishing moments is a set of polynomial equations in $\mathbf{x}$. We substitute $\mathbf{x}$ with $\mathbf{x}_k+\boldsymbol{\delta}_{\mathbf{x}}$. Provided that $\|\boldsymbol{\delta}_{\mathbf{x}}\|$ is small, the quadratic and higher-order terms in $\boldsymbol{\delta}_{\mathbf{x}}$ can be neglected, and these polynomial equations can be approximated by the linear system

$$\mathbf{A}_k\boldsymbol{\delta}_{\mathbf{x}} = \mathbf{b}_k. \tag{68}$$

In this way, the filter bank constructed with lifting-filter coefficients $\mathbf{x}_k+\boldsymbol{\delta}_{\mathbf{x}}$ has the desired vanishing-moment properties. Due to the problem formulation, the moments of interest are only guaranteed to be small, but not exactly zero. In practice, however, the moments are typically very close to zero, as will be illustrated later via our design examples.

Now we consider the frequency response of the highpass analysis filter H_1. The weighted error function e_{h_1} is defined in (39). In order to have good frequency selectivity, the function e_{h_1} must satisfy the constraint (40). From (8), $\widehat{h}_{1a}(\boldsymbol{\omega})$ has at least a second-order term in $\mathbf{x}$. Therefore, e_{h_1} is at least a fourth-order polynomial in $\mathbf{x}$. Using a similar approach as above, we replace $\mathbf{x}$ by $\mathbf{x}_k+\boldsymbol{\delta}_{\mathbf{x}}$ in $\widehat{h}_{1a}(\boldsymbol{\omega})$ with $\|\boldsymbol{\delta}_{\mathbf{x}}\|$ being small, and neglect the second- and higher-order terms in $\boldsymbol{\delta}_{\mathbf{x}}$. Now, $\widehat{h}_{1a}(\boldsymbol{\omega})$ is approximated by a linear function of $\boldsymbol{\delta}_{\mathbf{x}}$. Using (39), a quadratic approximation of e_{h_1} is obtained as

$$e_{h_1} = \boldsymbol{\delta}_{\mathbf{x}}^T\mathbf{H}_k\boldsymbol{\delta}_{\mathbf{x}} + \boldsymbol{\delta}_{\mathbf{x}}^T\mathbf{s}_k + c_k, \tag{69}$$

where $\mathbf{H}_k$ is a symmetric positive semidefinite matrix, and $\mathbf{H}_k$, $\mathbf{s}_k$, and c_k are dependent on $\mathbf{x}_k$. Therefore, the constraint $e_{h_1} \le \delta_{h_1}$ can be expressed in the form of a second-order cone constraint as

$$\left\|\widetilde{\mathbf{H}}_k\boldsymbol{\delta}_{\mathbf{x}} + \widetilde{\mathbf{s}}_k\right\|^2 \le \delta_{h_1} - \widetilde{c}_k. \tag{70}$$

Note that the approximation is not applied to e_{h_1}, but to $\widehat{h}_{1a}(\boldsymbol{\omega})$. In this way, the matrix $\mathbf{H}_k$ is guaranteed to be positive semidefinite, which allows for the form of a second-order cone as in (70).

Based on the preceding approximation methods of the vanishing-moment condition and frequency response constraint, the design of filter banks with more than two lifting steps can be formulated as an iterative SOCP problem. To solve this design problem, we use a scheme similar to Algorithm 1. Let K be the number of lifting steps. The modified algorithm (Algorithm 2) is given.

Upon termination of Algorithm 2, the output $\mathbf{x}^*$ will correspond to a filter bank with all of the desired properties. In Step (2), we deal with the constant δ_{h_1} in the same way as in Algorithm 1 (i.e., δ_{h_1} is chosen to be a scaled version of the error function evaluated at the point $\mathbf{x}_k$). We use a variable scaling factor D in the frequency response error function (39) since the Nyquist gain of H_1 is dependent on the lifting-filter coefficients in this case. For the kth iteration, we choose D to be the Nyquist gain of the highpass analysis filter obtained from the previous iteration (i.e., $D = \widehat{h}_{1a}(\pi,\pi)$ with $\widehat{h}_{1a}(\boldsymbol{\omega})$ being the signed amplitude response of H_1 obtained from the $(k-1)$th iteration).

Due to the linear approximation (68), the moments associated with the desired vanishing-moment conditions are only guaranteed to be small but not necessarily zero. An adjustment step can be applied after Step (3) to further reduce the moments in question at the expense of a slight decrease in the coding gain. This step is formulated as follows. Let $\{\Gamma_i(\mathbf{x})\} = 0$ be the set of polynomial equations that the lifting-filter coefficient vector $\mathbf{x}$ needs to satisfy to achieve N primal and $\widetilde{N}$ dual vanishing moments. When $\|\boldsymbol{\delta}_{\mathbf{x}}\|$ is small,

This iterative algorithm consists of the following steps (where k denotes the iteration number indexed from zero).

Step (1)

Select an initial point $\mathbf{x}_0$ such that the resulting filter bank has the desired number of vanishing moments. We can choose the first two lifting filters using the method proposed for the two-lifting-step case, and then set the coefficients of the other $K-2$ lifting filters to be all zeros. Alternatively, we can randomly select the coefficients of the first $K-2$ filters, and then use the last two lifting filters to provide dual and primal vanishing moments. In this way, the filter bank constructed with the initial point $\mathbf{x}_0$ has the desired number of vanishing moments. Moreover, since the upper bound δ_{h_1} for the frequency response error function is chosen in the same way as in Algorithm 1, the frequency response constraint will not be violated. Therefore, $\mathbf{x}_0$ is inside the feasible region.

Step (2)

For the kth iteration, at the point $\mathbf{x}_k$, compute the gradient $\mathbf{g}$ of $G(\mathbf{x})$, $\mathbf{A}_k$ and $\mathbf{b}_k$ in (68), and $\widetilde{\mathbf{H}}_k$, $\widetilde{\mathbf{s}}_k$, and $\widetilde{c}_k$ in (70). Then, solve the SOCP problem:

$$\begin{aligned} &\text{minimize } \mathbf{g}^T\boldsymbol{\delta}_{\mathbf{x}} \\ &\text{subject to } \mathbf{A}_k\boldsymbol{\delta}_{\mathbf{x}} = \mathbf{b}_k, \\ &\left\|\widetilde{\mathbf{H}}_k\boldsymbol{\delta}_{\mathbf{x}} + \widetilde{\mathbf{s}}_k\right\| \le \sqrt{\delta_{h_1} - \widetilde{c}_k}, \\ &\|\boldsymbol{\delta}_{\mathbf{x}}\| \le \beta. \end{aligned} \tag{$p2$}$$

The linear constraint $\mathbf{A}_k\boldsymbol{\delta}_{\mathbf{x}} = \mathbf{b}_k$ can be parameterized as in Algorithm 1 to reduce the number of design variables, or be approximated by the second-order cone $\|\mathbf{A}_k\boldsymbol{\delta}_{\mathbf{x}} - \mathbf{b}_k\| \le \varepsilon_\delta$ with ε_δ being a prescribed tolerance. Then, we can use the optimal solution $\boldsymbol{\delta}_{\mathbf{x}}$ to update $\mathbf{x}_k$ by $\mathbf{x}_{k+1} = \mathbf{x}_k + \boldsymbol{\delta}_{\mathbf{x}}$. We can also optionally incorporate a line search into this process to improve the efficiency of the algorithm.

Step (3)

If $|G(\mathbf{x}_{k+1}) - G(\mathbf{x}_k)| < \varepsilon$, then output $\mathbf{x}^* = \mathbf{x}_{k+1}$ and stop. Otherwise, go to Step (2).

Algorithm 2: More-than-two lifting-step case.

the linear approximation of $\Gamma_i(\mathbf{x}^* + \boldsymbol{\delta}_\mathbf{x})$ is obtained by

$$\Gamma_i(\mathbf{x}^* + \boldsymbol{\delta}_\mathbf{x}) = \Gamma_i(\mathbf{x}^*) + \mathbf{g}_i^T \boldsymbol{\delta}_\mathbf{x}, \tag{71}$$

where $\mathbf{g}_i$ is the gradient of Γ_i at the point $\mathbf{x}^*$. This adjustment process can then be formulated as the following optimization problem:

$$\begin{aligned} &\text{minimize } \sum_i \left[\Gamma_i(\mathbf{x}^*) + \mathbf{g}_i^T \boldsymbol{\delta}_\mathbf{x}\right]^2 \\ &\text{subject to } ||\boldsymbol{\delta}_\mathbf{x}|| \le \beta_a, \end{aligned} \tag{72}$$

where β_a is a prescribed small value. The objective function of (72) can be rewritten as

$$\begin{aligned} &\sum_i \left(\Gamma_i(\mathbf{x}^*) + \mathbf{g}_i^T \boldsymbol{\delta}_\mathbf{x}\right)^2 \\ &\quad = \boldsymbol{\delta}_\mathbf{x}^T \left(\sum_i \mathbf{g}_i \mathbf{g}_i^T\right) \boldsymbol{\delta}_\mathbf{x} + \boldsymbol{\delta}_\mathbf{x}^T \left[2 \sum_i \Gamma_i(\mathbf{x}^*) \mathbf{g}_i\right] + \sum_i \Gamma_i^2(\mathbf{x}^*). \end{aligned} \tag{73}$$

Since $\sum_i \mathbf{g}_i \mathbf{g}_i^T$ is positive semidefinite, the objective function can be expressed in the form $\|\widetilde{\mathbf{H}}_{\boldsymbol{\delta}} \boldsymbol{\delta}_\mathbf{x} + \widetilde{\mathbf{s}}_{\boldsymbol{\delta}}\|^2 + \widetilde{c}_{\boldsymbol{\delta}}$. If we introduce another variable η to be the upper bound of the term $\|\widetilde{\mathbf{H}}_{\boldsymbol{\delta}} \boldsymbol{\delta}_\mathbf{x} + \widetilde{\mathbf{s}}_{\boldsymbol{\delta}}\|$, the problem in (72) becomes

$$\begin{aligned} &\text{minimize } \eta \\ &\text{subject to } ||\widetilde{\mathbf{H}}_{\boldsymbol{\delta}} \boldsymbol{\delta}_\mathbf{x} + \widetilde{\mathbf{s}}_{\boldsymbol{\delta}}|| \le \eta, \\ &\qquad ||\boldsymbol{\delta}_\mathbf{x}|| \le \beta_a. \end{aligned} \tag{74}$$

The above problem is equivalent to the SOCP problem,

$$\begin{aligned} &\text{minimize } \mathbf{f}^T \widetilde{\boldsymbol{\delta}}_\mathbf{x} \\ &\text{subject to } ||\widetilde{\widetilde{\mathbf{H}}}_{\boldsymbol{\delta}} \boldsymbol{\delta}_\mathbf{x} + \widetilde{\mathbf{s}}_{\boldsymbol{\delta}}|| \le \mathbf{f}^T \widetilde{\boldsymbol{\delta}}_\mathbf{x}, \\ &\qquad ||\widetilde{\mathbf{I}} \boldsymbol{\delta}_\mathbf{x}|| \le \beta_a, \end{aligned} \tag{75}$$

where $\widetilde{\boldsymbol{\delta}}_{\boldsymbol{\phi}} = [\eta \;\; \boldsymbol{\delta}_{\boldsymbol{\phi}}]^T$, $\mathbf{f} = [1 \;\; 0 \;\; \cdots \;\; 0]^T$, $\widetilde{\widetilde{\mathbf{H}}}_{\boldsymbol{\delta}} = [\mathbf{0} \;\; \widetilde{\mathbf{H}}_{\boldsymbol{\delta}}]$, and $\widetilde{\mathbf{I}} = [\mathbf{0} \;\; \mathbf{I}]$.

In Algorithm 2, instead of using the linear approximation (67) of the coding gain function G, we can also employ the quadratic approximation of G given by

$$G(\mathbf{x} + \boldsymbol{\delta}_\mathbf{x}) \approx G(\mathbf{x}) + \mathbf{g}^T \boldsymbol{\delta}_\mathbf{x} + \frac{1}{2} \boldsymbol{\delta}_\mathbf{x}^T \mathbf{Q} \boldsymbol{\delta}_\mathbf{x}, \tag{76}$$

where $\mathbf{g}$ and $\mathbf{Q}$ are the gradient and the Hessian of $G(\mathbf{x})$ at the point $\mathbf{x}$, respectively. A change similar to that used in Section 5.5 can be made to the SOCP problem ($p2$) in Step (2) of Algorithm 2.

The approximation method for the frequency response constraint explained previously in this section can also be used to control the frequency response of the lowpass analysis filter H_0 for filter banks with two or more lifting steps. For example, in the two-lifting-step case, the analysis lowpass filter frequency response $\widehat{h}_0(\boldsymbol{\omega})$ is a quadratic polynomial in the design vector $\boldsymbol{\phi}$. We can replace $\boldsymbol{\phi}$ by $\boldsymbol{\phi}_k + \boldsymbol{\delta}_{\boldsymbol{\phi}}$ in $\widehat{h}_0(\boldsymbol{\omega})$ and keep only the constant and first-order terms. Then, the error function e_{h_0} computed with this linear approximation of $\widehat{h}_0(\boldsymbol{\omega})$ becomes a quadratic function of $\boldsymbol{\delta}_{\boldsymbol{\phi}}$, and the constraint $e_{h_0} \le \delta_{h_0}$ can be expressed as a second-order cone in $\boldsymbol{\delta}_{\boldsymbol{\phi}}$.

7. DESIGN EXAMPLES

In order to demonstrate the effectiveness of our proposed design methods, we now present several examples of filter banks constructed using Algorithms 1 and 2. In passing, we note that our software implementation of these algorithms (written in MATLAB) is available on the Internet [31]. For all of the design examples in this section, the optimization is carried out for maximal coding gain assuming an isotropic image model with correlation coefficient $\rho = 0.95$ and a six-level wavelet decomposition.

Using our proposed methods, we designed three filter banks, henceforth referred to by the names OPT1, OPT3, and OPT4. The lifting-filter coefficient vectors $\{\mathbf{a}_i\}$ (as defined in (10) and (15)) for these three filter banks are given in Table 2. For comparison purposes, we also consider four filter banks produced using methods previously proposed by others, with three being quincunx and one being separable. The first two quincunx filter banks are constructed using the technique of [18], and are henceforth referred to by the names KS1 and KS2. The third quincunx filter bank is the so-called (6, 2) filter bank proposed in [9], which we henceforth refer to by the name G62. The one separable filter bank considered herein is the well-known 9/7 filter bank employed in the JPEG-2000 standard [1]. Some important characteristics of the various filter banks are shown in Table 3. The OPT1 filter bank was designed using Algorithm 1 with two lifting steps. The next two filter banks, referred to as OPT3 and OPT4, were designed using Algorithm 2 with three or more lifting steps, and thus, the desired vanishing-moment conditions are only guaranteed to be met approximately (i.e., the moments in question are only guaranteed to be close to zero). For each of these two filter banks, the order of the largest nonzero moment (of those in question) is shown in the rightmost column of Table 3. The frequency responses of the analysis and synthesis lowpass filters are shown in Figures 7, 8, and 9. Since the highpass filter frequency responses are simply modulated versions of the lowpass ones, the former have been omitted here due to space constraints. The primal scaling and wavelet functions are illustrated in Figures 10, 11, and 12.

From Table 3, clearly, the optimal designs, OPT1, OPT3, and OPT4, each have a higher isotropic coding gain than the KS1, KS2, and G62 quincunx filter banks. Furthermore, the designs with three and four lifting steps also have a higher isotropic coding gain than the 9/7 filter bank, which is very impressive considering that the 9/7 filter bank is well known for its high coding gain. For OPT3 and OPT4, the zeroth moments are nearly vanishing on the order of 10^{-10} to 10^{-12}, which is small enough to be considered as zero for all practical purposes. The first moments are automatically zero due to the linear-phase property as previously

Table 2: Lifting-filter coefficients for the (a) OPT1, (b) OPT3, and (c) OPT4 filter banks (where the coefficient vectors $\{\mathbf{a}_i\}$ are as defined in (10) and (15))

(a)

$\mathbf{a}_1$	$\mathbf{a}_2$
−0.0159198316	0.0141419383
0.0570315087	−0.0475750610
−0.3319070666	0.1826552865
−0.3336501890	0.1839773572
0.0596966372	−0.0501021101
−0.0177016160	0.0165757568
0	0
−0.0002158944	0.0073072183
0.0584826734	−0.0487234955
0.0590711965	−0.0488388947
−0.0014144431	0.0082567802
0	0
0	0
0	0
−0.0171945340	0.0165064152
−0.0162784411	0.0158188087
0	0
0	0

(b)

$\mathbf{a}_1$	$\mathbf{a}_2$	$\mathbf{a}_3$
0.0121916538	−0.0412467652	0.0312090846
−0.2252324567	0.2230448713	−0.1065049947
−0.2244562781	0.2234323639	−0.1060172665
0.0131716139	−0.0423652185	0.0301113988
0	0	0
0.0123383222	−0.0429058837	0.0289842780
0.0125969226	−0.0419932594	0.0317300494
0	0	0

(c)

$\mathbf{a}_1$	$\mathbf{a}_2$
0.0634983772	−0.0451377582
−0.1474840240	0.0687594491
−0.2023765008	0.1518386544
0.0294352099	−0.0326419204
0	0
0.0622324334	−0.0460766038
0.0202133422	−0.0240443429
0	0
$\mathbf{a}_3$	$\mathbf{a}_4$
−0.2321916679	0.2012955400
−0.0651787971	0.0186944256

discussed in Section 6.1. Lastly, from Figures 7 to 12, we see that the optimal filter banks have good diamond-shaped passbands/stopbands and smooth primal scaling and wavelet functions.

8. IMAGE CODING RESULTS AND ANALYSIS

In order to further demonstrate the utility of our new filter banks, they were employed in an enhanced version of the embedded lossy/lossless image codec of [32]. This codec can be used with either nonseparable or separable filter banks based on the lifting framework. Some additional information about the codec is included in the appendix. For test data, all twenty seven (reasonably sized) grayscale images from the JPEG-2000 test set [33] were used in our experiments.

Using each of the filter banks listed in Table 3, the test images were coded in a lossy manner at four compression ratios (i.e., 128, 64, 32, and 16), and then decoded. In each case, the difference between original and reconstructed images was measured in terms of PSNR. In the cases of quincunx and separable filter banks, six and three levels of decomposition were employed, respectively.

A statistical summary of all of the lossy compression results (i.e., for the twenty seven test images coded at four compression ratios) obtained with the quincunx filter banks is provided in Table 4. In particular, the table shows the percentage of cases where the OPT1, OPT3, and OPT4 optimal designs outperform the KS1, KS2, and G62 filter banks. We can see that our new filter banks outperform KS1 in 70% to 80% of the cases, outperform KS2 in more than 80% of the cases, and outperform G62 in more than 90% of the cases. It is worth noting that the KS1 filter bank has the best performance among all of the quincunx filter banks constructed using the method in [18] with filter supports comparable to our design examples, and the G62 filter bank has the best performance among the three filter banks in [9]. In other words, we are comparing our optimal designs to the very best competing quincunx filter banks produced by other methods.

For illustrative purposes, we now provide a subset of the lossy coding results, namely those obtained for the test images sar2 and gold. Information about these two images is provided in Table 5. The sar2 image is more isotropic (than separable) in nature, while the gold image is more separable, as demonstrated by the contour plots of their normalized autocorrelation functions shown in Figure 13. The lossy coding results for the sar2 and gold images are shown in Table 6. Obviously, our three optimal designs (i.e., OPT1, OPT3, and OPT4) perform very well, consistently outperforming the KS1, KS2, and G62 quincunx filter banks in all cases. For example, in the case of the sar2 image at a compression ratio of 16, our optimal designs outperform the KS1, KS2, and G62 filter banks by margins of 0.12 to 0.23, 0.29 to 0.4, and 0.42 to 0.53 dB, respectively. Moreover, for the isotropic sar2 image, our optimal designs even achieve better results than the 9/7 filter bank in most cases. For example, the OPT3 design outperforms the 9/7 filter bank at all of the four compression ratios considered (for the sar2 image). This is quite an encouraging result, as the 9/7 filter bank is generally held to be one of the very best in the literature.[1]

The reconstructed images associated with the optimal filter banks also have subjective quality comparable to that of

[1] Of course, the idea that nonseparable filter banks can offer improved performance (over separable ones) for images with nonseparable (e.g., isotropic) statistics is not a new one. In fact, it is this very idea that has inspired much research in the area of nonseparable filter banks. For example, this idea has been expressed in [21] as well as in many other works.

Table 3: Comparison of filter-bank characteristics.

Name	Support of lifting filters†	Support of analysis filters		Coding gain (dB)		Vanishing moments		
		Lowpass	Highpass	Isotropic	Separable	$\tilde{N}$	N	Max.
OPT1	$6 \times 6, 6 \times 6$	13×13	7×7	12.06	13.59	2	2	—
OPT3	$4 \times 4, 4 \times 4, 4 \times 4$	9×9	13×13	12.23	13.26	2	2	10^{-12}
OPT4	$4 \times 4, 4 \times 4, 2 \times 2, 2 \times 2$	13×13	11×11	12.21	13.07	2	2	10^{-10}
KS1	$6 \times 6, 6 \times 6$	13×13	7×7	11.95	13.64	6	6	—
KS2	$8 \times 8, 4 \times 4$	15×15	11×11	11.75	13.92	8	4	—
G62	$6 \times 6, 2 \times 2$	13×13	11×11	11.64	12.98	6	2	—
9/7	2, 2, 2, 2	9	7	12.09	14.88	4	4	—

† Support regions are diamond-shaped for OPT1, OPT3, OPT4, KS1, and KS2, and rectangular-shaped for G62.

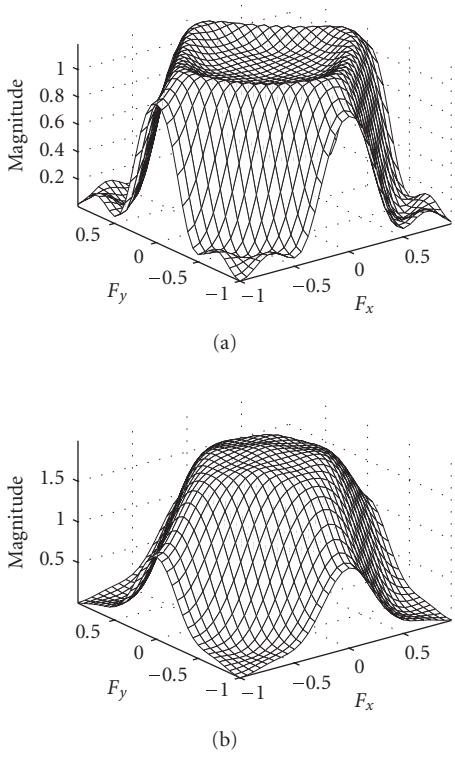

Figure 7: Frequency responses of the (a) lowpass analysis and (b) lowpass synthesis filters of OPT1.

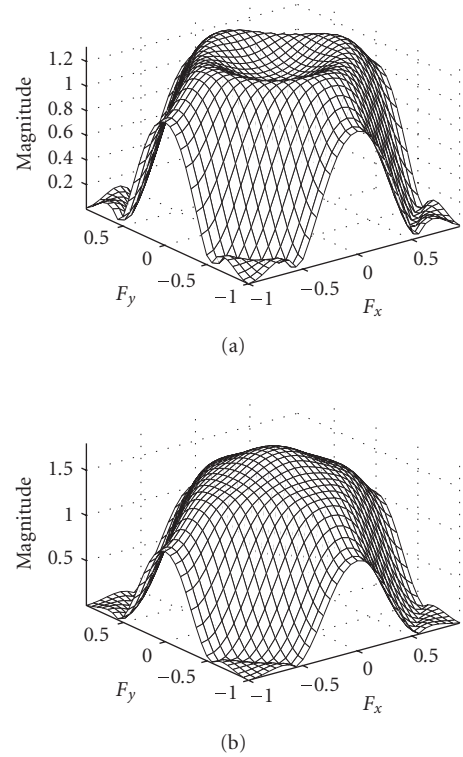

Figure 8: Frequency responses of the (a) lowpass analysis and (b) lowpass synthesis filters of OPT3.

the KS1, KS2, G62, and 9/7 filter banks. As an example, the lossy reconstructed images for sar2 using these filter banks are shown in Figure 14. It is apparent from the figures that the reconstructed images corresponding to OPT1, OPT3, and OPT4 have good subjective quality.

9. CONCLUSIONS

In this paper, we have proposed two new optimization-based methods (and variations thereof) for the design of quincunx filter banks for image coding. The proposed design techniques (i.e., Algorithms 1 and 2) yield linear-phase PR systems with high coding gain, good frequency selectivity, and certain prescribed vanishing-moment properties.

Using Algorithms 1 and 2, we designed several filter banks with all of the desirable properties. These optimal filter banks were employed in an image codec and their coding performance was compared to that of four previously proposed filter banks (three quincunx and one separable). The experimental results show that our new filter banks outperform the three previously proposed quincunx filter banks in 72% to 95% of the test cases. Thus, our design methods

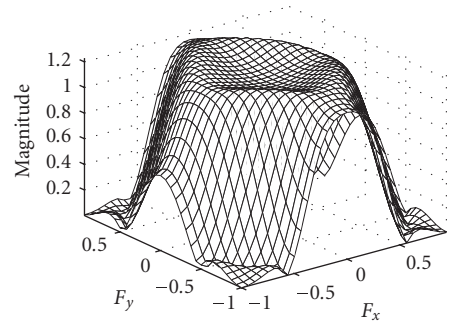

(a)

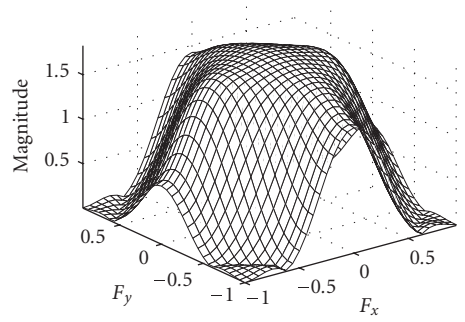

(b)

Figure 9: Frequency responses of the (a) lowpass analysis and (b) lowpass synthesis filters of OPT4.

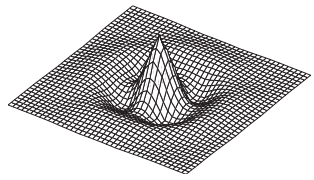

(a)

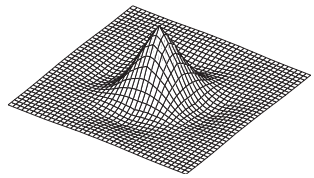

(b)

Figure 10: The (a) primal wavelet and (b) primal scaling functions for OPT1.

clearly yield superior filter banks compared to other quincunx filter-bank design methods. Moreover, in some cases, our optimal designs even outperform the (separable) 9/7 filter bank, which is considered to be one of the very best in the literature. These results demonstrate the effectiveness of our new design techniques. Furthermore, through the use of our design methods, it is possible to develop higher-performance image codecs based on quincunx filter banks.

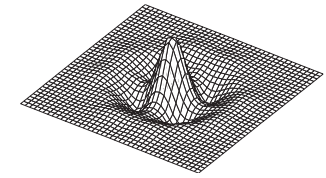

(a)

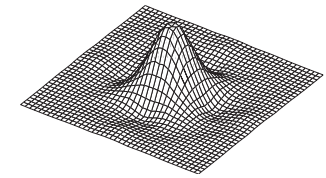

(b)

Figure 11: The (a) primal wavelet and (b) primal scaling functions for OPT3.

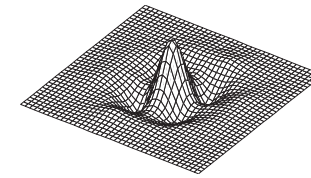

(a)

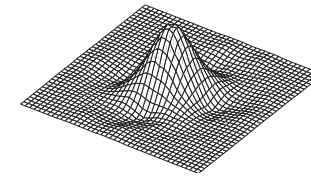

(b)

Figure 12: The (a) primal wavelet and (b) primal scaling functions for OPT4.

Table 4: Statistical summary of the lossy compression results for twenty seven test images, each coded at compression ratios of 128, 64, 32, and 16. Percentage of cases where the OPT1, OPT3, and OPT4 optimal designs outperform the KS1, KS2, and G62 (quincunx) filter banks.

Filter banks	OPT1	OPT3	OPT4
KS1	78%	75%	72%
KS2	83%	82%	81%
G62	95%	94%	93%

Table 5: Small subset of test images.

Image	Size	bpp	Model	Description
sar2	800×800	12	Isotropic	Synthetic aperture radar
gold	720×576	8	Separable	Houses

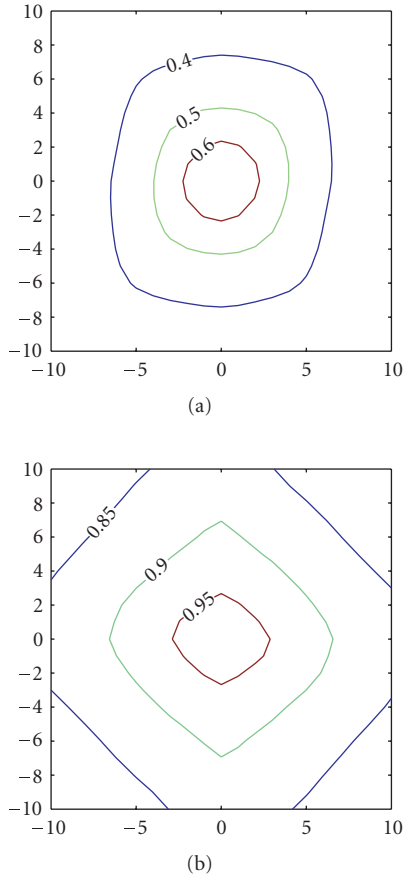

Figure 13: The contour plots of the autocorrelation functions of the (a) sar2 and (b) gold images.

Table 6: Lossy compression results for the (a) sar2 and (b) gold images.

(a)

CR†	PSNR (dB)						
	OPT1	OPT3	OPT4	KS1	KS2	G62	9/7
128	22.73	**22.77**	22.75	22.66	22.56	22.39	22.75
64	23.54	23.60	**23.61**	23.45	23.34	23.13	23.56
32	24.73	**24.82**	24.79	24.62	24.49	24.29	24.70
16	26.67	**26.78**	26.75	26.55	26.38	26.25	26.62

(b)

CR†	PSNR (dB)						
	OPT1	OPT3	OPT4	KS1	KS2	G62	9/7
128	27.14	**27.19**	27.12	26.98	26.92	26.72	27.16
64	28.90	28.95	28.95	28.82	28.71	28.47	**29.06**
32	30.90	30.97	30.95	30.81	30.70	30.50	**31.28**
16	33.36	33.41	33.35	33.28	33.17	32.97	**33.82**

†Compression ratio.

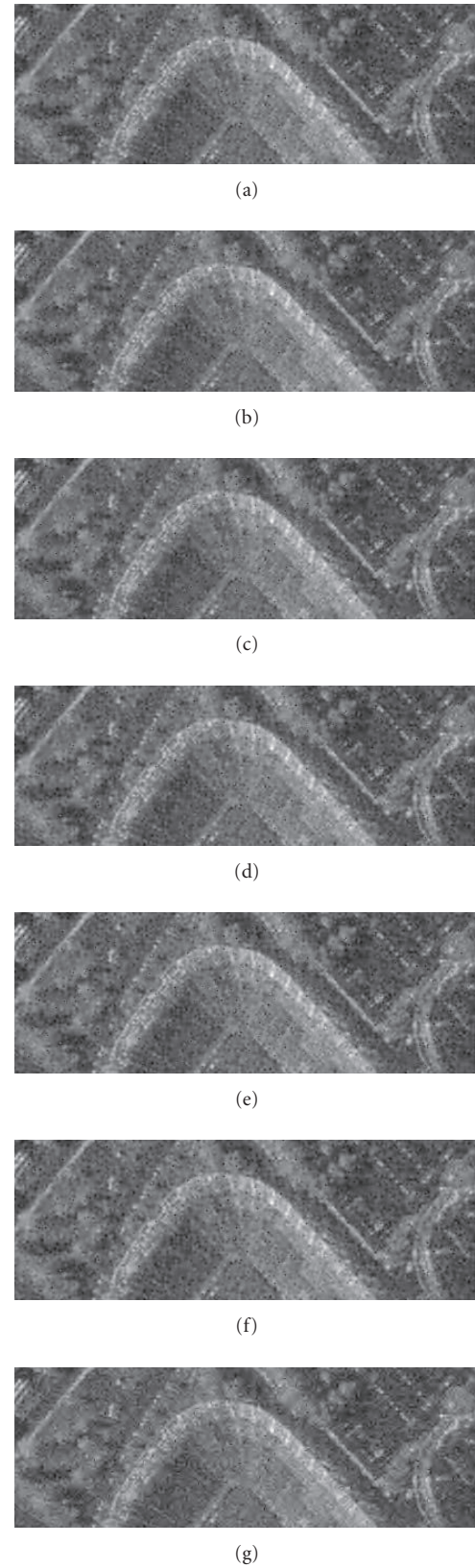

Figure 14: Part of the lossy reconstructions obtained for the sar2 image at a compression ratio of 32 using the (a) OPT1, (b) OPT3, (c) OPT4, (d) KS1, (e) KS2, (f) G62, and (g) 9/7 filter banks.

APPENDIX

IMAGE CODEC

The image codec [32] used for collecting experimental results herein was written in C++ and it supports both lossy and lossless compression of grayscale images. The codec was partly inspired by technologies contained in the JPEG-2000 Verification-Model 0.0 software [34]. Although originally developed in [32], the codec has undergone major changes since that time in order to improve its coding performance. The codec employs reversible integer-to-integer versions of wavelet transforms [25] (which can be trivially constructed from the lifting realization of a filter bank).

The general structure of the codec is as follows. In the encoder, a wavelet transform is first applied to the input data. Then, a bitplane coder is applied independently to each of the resulting subband signals. The bitplane coder employs three coding passes per bitplane (i.e., predicted significant, refinement, and predicted insignificant passes), similar in spirit to those found in the JPEG-2000 codec [1], for example. The symbols generated by the bitplane coder are then entropy-coded using a context-based adaptive arithmetic coder. The ordering of the data in the codestream is optimized for rate-distortion performance, and rate control is achieved solely by the truncation of the embedded codestream. The structure of the decoder essentially mirrors that of the encoder.

ACKNOWLEDGMENT

The authors would like to thank the anonymous reviewers for useful comments, which have helped to improve the quality of this paper.

REFERENCES

[1] ISO/IEC 15444-1, Information technology—JPEG 2000 image coding system—Part 1: Core coding system, 2000.

[2] D. B. H. Tay and N. G. Kingsbury, "Flexible design of multidimensional perfect reconstruction FIR 2-band filters using transformations of variables," *IEEE Transactions on Image Processing*, vol. 2, no. 4, pp. 466–480, 1993.

[3] P. P. Vaidyanathan, *Multirate Systems and Filter Banks*, Prentice Hall, Upper Saddle River, NJ, USA, 1993.

[4] T. Chen and P. P. Vaidyanathan, "Multidimensional multirate filters and filter banks derived from one-dimensional filters," *IEEE Transactions on Signal Processing*, vol. 41, no. 5, pp. 1749–1765, 1993.

[5] J. M. Shpairo, "Adaptive McClellan transformations for quincunx filter banks," *IEEE Transactions on Signal Processing*, vol. 42, no. 3, pp. 642–648, 1994.

[6] T. A. C. M. Kalker and I. A. Shah, "Group theoretic approach to multidimensional filter banks: theory and applications," *IEEE Transactions on Signal Processing*, vol. 44, no. 6, pp. 1392–1405, 1996.

[7] J. H. McClellan, "The design of two-dimensional digital filters by transformation," in *Proceedings of the 7th Annual Princeton Conference on Information Sciences and Systems*, pp. 247–251, Princeton, NJ, USA, March 1973.

[8] S.-M. Phoong, C. W. Kim, P. P. Vaidyanathan, and R. Ansari, "New class of two-channel biorthogonal filter banks and wavelet bases," *IEEE Transactions on Signal Processing*, vol. 43, no. 3, pp. 649–665, 1995.

[9] A. Gouze, M. Antonini, and M. Barlaud, "Quincunx lifting scheme for lossy image compression," in *Proceedings of the IEEE International Conference on Image Processing (ICIP '00)*, vol. 1, pp. 665–668, Vancouver, BC, Canada, September 2000.

[10] S. C. Chan, K. S. Pun, and K. L. Ho, "On the design and implementation of a class of multiplierless two-channel 1D and 2D nonseparable PR FIR filterbanks," in *Proceedings of the IEEE International Conference on Image Processing (ICIP '01)*, vol. 2, pp. 241–244, Thessaloniki, Greece, October 2001.

[11] K. S. C. Pun and T. Q. Nguyen, "A novel and efficient design of multidimensional PR two-channel filter banks with hourglass-shaped passband support," *IEEE Signal Processing Letters*, vol. 11, no. 3, pp. 345–348, 2004.

[12] G. Karlsson and M. Vetterli, "Theory of two-dimensional multirate filter banks," *IEEE Transactions on Acoustics, Speech, and Signal Processing*, vol. 38, no. 6, pp. 925–937, 1990.

[13] E. Viscito and J. P. Allebach, "The analysis and design of multidimensional FIR perfect reconstruction filter banks for arbitrary sampling lattices," *IEEE Transactions on Circuits and Systems*, vol. 38, no. 1, pp. 29–41, 1991.

[14] T. D. Tran, R. L. de Queiroz, and T. Q. Nguyen, "Linear-phase perfect reconstruction filter bank: lattice structure, design, and application in image coding," *IEEE Transactions on Signal Processing*, vol. 48, no. 1, pp. 133–147, 2000.

[15] W. Sweldens, "The lifting scheme: a custom-design construction of biorthogonal wavelets," *Applied and Computational Harmonic Analysis*, vol. 3, no. 2, pp. 186–200, 1996.

[16] I. Daubechies and W. Sweldens, "Factoring wavelet transforms into lifting steps," *Journal of Fourier Analysis and Applications*, vol. 4, no. 3, pp. 247–268, 1998.

[17] T. Cooklev, A. Nishihara, T. Yoshida, and M. Sablatash, "Multidimensional two-channel linear phase FIR filter banks and wavelet bases with vanishing moments," *Multidimensional Systems and Signal Processing*, vol. 9, no. 1, pp. 39–76, 1998.

[18] J. Kovačević and W. Sweldens, "Wavelet families of increasing order in arbitrary dimensions," *IEEE Transactions on Image Processing*, vol. 9, no. 3, pp. 480–496, 2000.

[19] J. Zhou, M. N. Do, and J. Kovačević, "Multidimensional orthogonal filter bank characterization and design using the Cayley transform," *IEEE Transactions on Image Processing*, vol. 14, no. 6, pp. 760–769, 2005.

[20] J. Zhou, M. N. Do, and J. Kovačević, "Special paraunitary matrices, Cayley transform, and multidimensional orthogonal filter banks," *IEEE Transactions on Image Processing*, vol. 15, no. 2, pp. 511–519, 2006.

[21] M. Feilner, D. Van De Ville, and M. Unser, "An orthogonal family of quincunx wavelets with continuously adjustable order," *IEEE Transactions on Image Processing*, vol. 14, no. 4, pp. 499–510, 2005.

[22] D. Van De Ville, T. Blu, and M. Unser, "Isotropic polyharmonic B-splines: scaling functions and wavelets," *IEEE Transactions on Image Processing*, vol. 14, no. 11, pp. 1798–1813, 2005.

[23] J. Kovačević and M. Vetterli, "Nonseparable multidimensional perfect reconstruction filter banks and wavelet bases for $\mathbb{R}^n$," *IEEE Transactions on Information Theory*, vol. 38, no. 2, part 2, pp. 533–555, 1992.

[24] T. T. Nguyen and S. Oraintara, "Multiresolution direction filterbanks: theory, design, and applications," *IEEE Transactions on Signal Processing*, vol. 53, no. 10, pp. 3895–3905, 2005.

[25] A. R. Calderbank, I. Daubechies, W. Sweldens, and B.-L. Yeo, "Wavelet transforms that map integers to integers," *Applied*

and Computational Harmonic Analysis, vol. 5, no. 3, pp. 332–369, 1998.
[26] Y. Chen, "Design and application of quincunx filter banks," M.S. thesis, Department of Electrical and Computing Engineering, University of Victoria, Victoria, BC, Canada, 2006.
[27] J. Katto and Y. Yasuda, "Performance evaluation of subband coding and optimization of its filter coefficients," in *Visual Communications and Image Processing (VCIP '91)*, vol. 1605 of *Proceedings of SPIE*, pp. 95–106, Boston, Mass, USA, November 1991.
[28] M. Vetterli, J. Kovačević, and D. J. Legall, "Perfect reconstruction filter banks for HDTV representation and coding," *Signal Processing: Image Communication*, vol. 2, no. 3, pp. 349–363, 1990.
[29] M. S. Lobo, L. Vandenberghe, S. Boyd, and H. Lebret, "Applications of second-order cone programming," *Linear Algebra and Its Applications*, vol. 284, no. 1–3, pp. 193–228, 1998.
[30] J. F. Sturm, "Using SeDuMi 1.02, a MATLAB toolbox for optimization over symmetric cones," *Optimization Methods and Software*, vol. 11, no. 1, pp. 625–653, 1999.
[31] Michael Adams', August 2006 http://www.ece.uvic.ca/~mdadams.
[32] M. D. Adams, "ELEC 545 project: a wavelet-based lossy/ lossless image compression system," Department of Electrical and Computer Engineering, University of British Columbia, Vancouver, BC, Canada, April 1999.
[33] "JPEG-2000 test images," ISO/IEC JTC 1/SC 29/WG 1 N 545, July 1997.
[34] SAIC and University of Arizona, "JPEG-2000 VM 0 software", ISO/IEC JTC 1/SC 29/WG 1 N 840, May 1998.

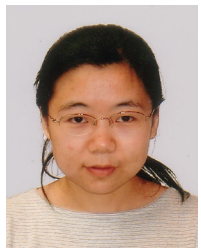

Yi Chen received the B.Eng. degree in electronic engineering from Tsinghua University, Beijing, China, in 2002, and the M.A.Sc. degree in electrical engineering from the University of Victoria, Victoria, BC, Canada, in 2006. Her research interests include image processing, wavelets, and multirate systems.

Michael D. Adams received the B.A.Sc. degree in computer engineering from the University of Waterloo, Waterloo, ON, Canada, in 1993, the M.A.Sc. degree in electrical engineering from the University of Victoria, Victoria, BC, Canada, in 1998, and the Ph.D. degree in electrical engineering from the University of British Columbia, Vancouver, BC, Canada, in 2002. Since 2003, he has been an Assistant Professor in the Department of Electrical and Computer Engineering at the University of Victoria. From 1993 to 1995, he was a member of technical staff at Bell-Northern Research (now Nortel Networks) in Ottawa, ON, Canada. His research interests include digital signal processing, wavelets, multirate systems, image coding, and multimedia systems. He is the recipient of a Natural Sciences and Engineering Research Council (of Canada) Postgraduate Scholarship. He is a voting member of the Canadian Delegation to ISO/IEC JTC 1/SC 29 (i.e., Coding of Audio, Picture, Multimedia and Hypermedia Information), and has been an active participant in the JPEG-2000 standardization effort, serving as Coeditor of the JPEG-2000 Part-5 standard and principal author of one of the first JPEG-2000 implementations (i.e., JasPer). He is also a Member of the IEEE and a registered Professional Engineer in the province of British Columbia.

Wu-Sheng Lu received the B.S. degree in mathematics from Fudan University, Shanghai, China, in 1964, and the M.S. degree in electrical engineering and the Ph.D. degree in control science from the University of Minnesota, Minn, USA, in 1983 and 1984, respectively. He was a Postdoctoral Fellow at the University of Victoria, Victoria, BC, Canada, in 1985 and a visiting Assistant Professor with the University of Minnesota in 1986. Since 1987, he has been with the University of Victoria where he is a Professor. His current teaching and research interests are in the general areas of digital signal processing and application of optimization methods. He is the coauthor with A. Antoniou of *Two-Dimensional Digital Filters* (Marcel Dekker, 1992). He served as an Associate Editor of the Canadian Journal of Electrical and Computer Engineering in 1989, and Editor of the same journal from 1990 to 1992. He served as an Associate Editor for the IEEE Transactions on Circuits and Systems, Part II, from 1993 to 1995 and for Part I of the same journal from 1999 to 2001 and from 2004 to 2005. Presently he is serving as an Associate Editor for the International Journal of Multidimensional Systems and Signal Processing. He is a Fellow of the Engineering Institute of Canada and the IEEE.

EURASIP JOURNAL ON ADVANCES IN SIGNAL PROCESSING

Special Issue on Multihop-Based Cellular Networks

Call for Papers

The deployment of 3G cellular networks is intended to meet the rapidly increasing number of mobile subscribers and the growing demand for new high data rate services such as mobile Internet, video conferencing, and interactive gaming. With the anticipated growth rates in cellular communications, the demand is still likely to exceed the available resources. This fact necessitates research towards practical capacity/coverage enhancement and power reduction techniques for the evolution of cellular networks towards 4G.

Motivated by a growing number of applications, there has been recently elevated interest in the design of wireless ad hoc networks that do not depend on a fixed infrastructure where nodes communicate via multihop transmission. Multihop transmission can possibly lead to coverage extension, capacity enhancement, QoS improvement, and power reduction. Deploying wireless ad hoc network architectures for a large-scale personal wireless communication system in which any mobile station (MS) can communicate with its base station (BS) via an arbitrary number of hops may not be practically feasible. Therefore, it is prudent to combine the benefits of the centralized architecture of traditional wireless cellular networks with the distributed architecture of pure wireless ad hoc networks into a joint design that allows for controlled multihop transmissions in cellular networks. In multihop-based cellular networks, an MS which meets a predefined set of conditions, for example, is located in a specific area inside the cell or cannot establish a direct connection with the BS, will use other mobile or fixed stations as relays to communicate with its BS. To enable the successful and efficient integration of multihop transmission in cellular networks, there is an essential need for signal processing research to address a wide range of problems.

Original contributions are solicited related to all aspects of signal processing for multihop-based cellular networks. Topics of interest include, but are not limited to:

- Performance analysis
- Advanced antenna techniques
- Centralized and decentralized detection and estimation
- Distributed signal processing algorithms
- Cooperative diversity and coding techniques
- Cross-layer designs
- Resource allocation algorithms
- QoS support mechanisms
- Channel modeling
- Synchronization and localization
- Test bed design and experimental measurements

Authors should follow the EURASIP Journal on Advances in Signal Processing manuscript format described at http://www.hindawi.com/journals/asp/. Prospective authors should submit an electronic copy of their complete manuscript through the EURASIP Journal on Advances in Signal Processing Manuscript Tracking System at http://www.hindawi.com/mts/, according to the following timetable:

Manuscript Due	July 1, 2007
First Round of Reviews	November 1, 2007
Publication Date	February 1, 2008

Guest Editors:

Zaher Dawy, Department of Electrical and Computer Engineering, American University of Beirut, P.O. Box 11-0236, Bliss Street, Beirut 1107 2020, Lebanon; zaher.dawy@aub.edu.lb

Mischa Dohler, France Telecom R&D, 38243 Meylan, France; mischa.dohler@orange-ftgroup.com

Georgio B. Giannakis, Department of Electrical and Computer Engineering, University of Minnesota, Minneapolis, MN 55455-0167, USA; georgios@umn.edu

Jing Wang, School of Information Science and Technology, Tsinghua University, Beijing 100084, China; wangj@tsinghua.edu.cn

EURASIP JOURNAL ON ADVANCES IN SIGNAL PROCESSING

Special Issue on Wireless Cooperative Networks

Call for Papers

Motivations

Cooperative networks are gaining increasing interest from ICT society due to the capability of improving the performance of communication systems as well as providing a fertile environment for the development of context-aware services.

Cooperative communications and networking is a new communication paradigm involving both transmission and distributed processing promising significant increase of capacity and diversity gain in wireless networks, by counteracting faded channels with *cooperative diversity.*

On one hand, the integration of long-range and short-range wireless communication networks (e.g., infrastructured networks such as 3G, wireless ad hoc networks, and wireless sensor networks) improves the performance in terms of both area coverage and quality of service (indeed representing a form of diversity reflected in a greater capacity and number of potential users). On the other hand, the cooperation among heterogeneous nodes, as in the case of wireless sensor networks, allows a distributed space-time signal processing supporting, with a reduced complexity or energy consumption per node, environmental monitoring, localization techniques, distributed measurements, and so forth.

The relevance of this topic is also reflected by numerous sessions in current international conferences on the field as well as by the increasing number of national and international projects worldwide financed on these aspects.

List of topics

This issue tries to collect cutting-edge research achievements in this area. We solicit papers that present original and unpublished work on topics including, but not limited to, the following:

- Physical layer models, for example, channel models (statistics, fading, MIMO, feedback)
- Device constraints (power, energy, multiple access, synchronization) and resource management
- Distributed processing and resource management for cooperative networks, for example, distributed compression in wireless sensor networks, channel and network codes design
- Performance metrics, for example, capacity, cost, outage, delay, energy, scaling laws
- Cross-layer issues, for example, PHY/MAC/NET interactions, joint source-channel coding, separation theorems
- Multiterminal information theory
- Multihop communications
- Integration of wireless heterogeneous (long- and short-range) systems

Authors should follow the EURASIP JASP manuscript format described at http://www.hindawi.com/journals/asp/. Prospective authors should submit an electronic copy of their complete manuscript through the EURASIP JASP Manuscript Tracking System at http://www.hindawi.com/mts/, according to the following timetable:

Manuscript Due	November 1, 2007
First Round of Reviews	February 1, 2008
Publication Date	May 1, 2008

GUEST EDITORS:

Andrea Conti, Engineering Department in Ferrara (ENDIF), University of Ferrara, 44100 Ferrara, Italy; a.conti@ieee.org

Jiangzhou Wang, Department of Electronics, University of Kent, Canterbury, Kent CT2 7NT, UK; j.z.wang@kent.ac.uk

Hyundong Shin, Department of Radio Communication Engineering, School of Electronics and Information, Kyung Hee University, Gueonggi-Do 449-701, South Korea, Korea; hshin@khu.ac.kr

Ramesh Annavajjala, ArrayComm Inc., San Jose, CA 95131-1014, USA; ramesh.annavajjala@gmail.com

Moe Win, Department of Aeronautics and Astronautics, Massachusetts Institute of Technology, Cambridge, MA 02139, USA; moewin@mit.edu